iScience

CellPress
OPEN ACCESS

Article

FUS-dependent microRNA deregulations identify TRIB2 as a druggable target for ALS motor neurons

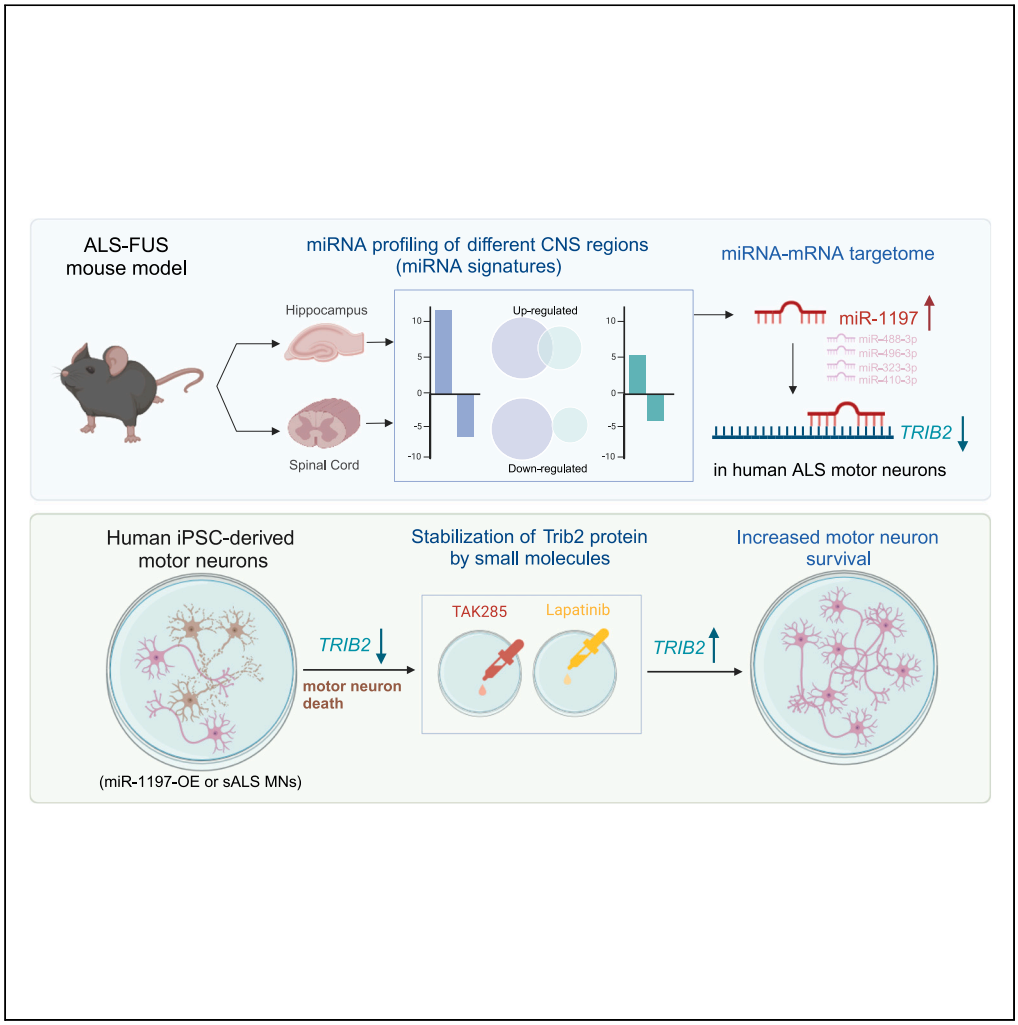

Wan Yun Ho, Li-Ling Chak, Jin-Hui Hor, ..., Shi-Yan Ng, Katsutomo Okamura, Shuo-Chien Ling

okamurak@bs.naist.jp (K.O.)
phsling@nus.edu.sg (S.-C.L.)

Highlights

miRNA profiling reveals miRNA signature in different CNS regions and ALS disease states

MiR-1197 targets the pro-survival pseudokinase Trib2 that is reduced in ALS motor neurons

Pharmacological stabilization of TRIB2 protein rescues the death of ALS motor neurons

miRNA profiling probes the molecular mechanisms underlying selective vulnerability

Ho et al., iScience *26*, 108152
November 17, 2023
https://doi.org/10.1016/j.isci.2023.108152

iScience

CellPress
OPEN ACCESS

Article

FUS-dependent microRNA deregulations identify TRIB2 as a druggable target for ALS motor neurons

Wan Yun Ho,[1,2,11] Li-Ling Chak,[1,3,11] Jin-Hui Hor,[4,11] Fujia Liu,[1,11] Sandra Diaz-Garcia,[5] Jer-Cherng Chang,[1] Emma Sanford,[1] Maria J. Rodriguez,[5] Durgadevi Alagappan,[1] Su Min Lim,[6] Yik-Lam Cho,[1] Yuji Shimizu,[7] Alfred Xuyang Sun,[2] Sheue-Houy Tyan,[5,8,12] Edward Koo,[1,5,8] Seung Hyun Kim,[6] John Ravits,[5] Shi-Yan Ng,[4] Katsutomo Okamura,[3,7,9,*] and Shuo-Chien Ling[1,2,10,13,*]

SUMMARY

MicroRNAs (miRNAs) modulate mRNA expression, and their deregulation contributes to various diseases including amyotrophic lateral sclerosis (ALS). As fused in sarcoma (FUS) is a causal gene for ALS and regulates biogenesis of miRNAs, we systematically analyzed the miRNA repertoires in spinal cords and hippocampi from ALS-FUS mice to understand how FUS-dependent miRNA deregulation contributes to ALS. miRNA profiling identified differentially expressed miRNAs between different central nervous system (CNS) regions as well as disease states. Among the up-regulated miRNAs, miR-1197 targets the pro-survival pseudokinase *Trib2*. A reduced *TRIB2* expression was observed in iPSC-derived motor neurons from ALS patients. Pharmacological stabilization of TRIB2 protein with a clinically approved cancer drug rescues the survival of iPSC-derived human motor neurons, including those from a sporadic ALS patient. Collectively, our data indicate that miRNA profiling can be used to probe the molecular mechanisms underlying selective vulnerability, and TRIB2 is a potential therapeutic target for ALS.

INTRODUCTION

Fused in sarcoma (FUS)/translocated in liposarcoma (TLS), hereafter referred as FUS, was originally identified as an oncogenic protein in various cancers when fused with different transcription factors from chromosome translocation.[1,2] In addition to its link to cancer, since 2009, over 40 mutations in FUS have been associated with two overlapping adult-onset neurodegenerative diseases: amyotrophic lateral sclerosis (ALS) and frontotemporal dementia (FTD).[3,4] Furthermore, pathological inclusions and cytosolic distribution of FUS are observed in ALS and FTD patients without FUS mutations,[5,6] suggesting that FUS dysfunctions may affect common pathogenic pathways leading to ALS and FTD. Clinically, ALS is characterized by progressive muscle wasting, weakness in limbs and the bulbar region, and eventual death with a severe degree of motor neuron degeneration. On the other hand, the FTDs are a group of neurodegenerative disorders featuring progressive deterioration of behavior or language and associated pathology in the frontal and temporal lobes. Although both diseases are phenotypically different, they shared genetic mutations and pathological inclusions, including FUS, thereby establishing ALS and FTD as a disease continuum.[7–9] Because hereditary (or familial) and sporadic form of ALS/FTD exhibit the same symptoms and share common pathological hallmarks,[10] disease-causing mutations in genes identified in hereditary form of disease are utilized to establish various *in vitro* and *in vivo* models. These include various genetically engineered organisms, ranging from yeast, *c. elegans*, *Drosophila*, Zebrafish, mouse, and non-human primates.[11,12] Furthermore, induced pluripotent stem cells (iPSCs) coupled with directed differentiation empower the use of patient-derived cells.[13] As such, elucidating the physiological and pathophysiological role of FUS could aid the understanding the underlying pathogenic processes and potential therapies for ALS and FTD.

[1]Department of Physiology, Yong Loo Lin School of Medicine, National University of Singapore, Singapore 117549, Singapore
[2]Programs in Neuroscience and Behavioral Disorders, Duke-NUS Medical School, Singapore 169857, Singapore
[3]Temasek Lifesciences Laboratory, Singapore 117604, Singapore
[4]Institute of Molecular and Cellular Biology, A*STAR Research Entities, 61 Biopolis Drive, Singapore 138673, Singapore
[5]Department of Neurosciences, University of California, San Diego, La Jolla, CA 92093, USA
[6]Department of Neurology, Biomedical Research Institute, Hanyang University College of Medicine, Seoul 04763, Republic of Korea
[7]Nara Institute of Science and Technology, 8916-5 Takayama, Ikoma, Nara 630-0192, Japan
[8]Department of Medicine, Yong Loo Lin School of Medicine, National University of Singapore, Singapore 117549, Singapore
[9]School of Biological Sciences, Nanyang Technological University, Singapore 639798, Singapore
[10]Healthy Longevity Translational Research Programme, Yong Loo Lin School of Medicine, National University of Singapore, Singapore 117549, Singapore
[11]These authors contribute equally
[12]deceased
[13]Lead contact
*Correspondence: okamurak@bs.naist.jp (K.O.), phsling@nus.edu.sg (S.-C.L.)
https://doi.org/10.1016/j.isci.2023.108152

FUS is a 526 amino acid protein containing a low complexity domain coupled with DNA/RNA-binding motifs.[14] FUS can bind to both single- and double-stranded nucleic acids, including non-coding RNAs, and regulate various biological functions.[3,7,15–17] In mRNA metabolism, FUS regulates the direction of transcription,[18] transcription-splicing coupling,[19,20] alternative splicing,[19,21,22] polyadenylation site selection,[23] and RNA localization and translation.[24–28] In addition, FUS also regulates a wide range of other non-coding RNA species, including RNAP III-transcribed small structural and catalytic RNAs,[29] long non-coding RNA,[30] miRNA,[31] and circular RNA.[32] FUS is also involved in DNA damage response,[33,34] where chromosome instability and increased radiation sensitivity was observed in cells lacking the FUS gene.[35–37] In summary, FUS is an important factor in the biogenesis and processing of coding and non-coding RNAs and in maintaining genomic integrity. Furthermore, ALS-linked mutations in FUS have been showed to disrupt intra-axonal translation[26] and affect mitochondrial functions by sequestering respiratory chain complex mRNAs.[38,39] Beyond mutations in the coding region, ALS-associated mutation in the 3′-UTR of FUS leading to FUS protein accumulation has been reported,[40] suggesting that FUS accumulation may be sufficient to cause ALS. A working model that has been supported by two independent mouse models.[41,42] Indeed, additional copy of "wild type" APP gene (encoding amyloid precursor protein) and SNCA (encoding α-synuclein) have been shown to be causal for Alzheimer's disease and Parkinson's disease, respectively,[43,44] further underscoring that elevated expression of disease-associate gene without mutation is sufficient to drive disease pathogenesis. Thus, it is critical to elucidating if, and if so, how any and/or more of the previous FUS-mediated processes may go awry and relevant to ALS and FTD pathogenesis.

MicroRNAs (miRNAs) are small (19–23 nucleotide-long) non-coding RNAs that modulate gene expression post-transcriptionally.[45,46] Currently, there are more than 2,500 annotated microRNAs in the human genome.[47,48] After transcription, primary miRNA transcripts (pri-miRNAs) are processed in a stepwise manner by two RNase III complexes, microprocessor in the nucleus and Dicer complex in the cytosol. The microprocessor complex generates precursor miRNA (pre-miRNA), which is subsequently exported to the cytosol for Dicer to process and generate mature miRNA.[45,46,48] Microprocessor is minimally comprised the ribonuclease Drosha and its double-stranded RNA-binding protein partner, DiGeorge syndrome chromosomal region 8 (DGCR8).[49,50] Various cofactors are reported to associate with microprocessor,[50,51] including DDX5/p68, and DDX17/p72 [50]. FUS has been shown to facilitate microRNA biogenesis by recruiting Drosha co-transcriptionally,[31] where it likely associates with components of the microprocessor complex.[50,52] Furthermore, FUS has been shown to facilitate optimal miR-mediated gene silencing by interacting with AGO2.[53] Altogether, these studies suggest that FUS is involved in regulating the biogenesis of miRNA and the effectiveness of miRNA actions.

Given the known function of FUS in miRNA processing,[31] we hypothesized that FUS-mediated miRNA dysfunctions may play a role in motor neuron damage. If so, miRNA signatures and their associated targets could be used to investigate the underlying pathogenic mechanisms. To test this, we took an unbiased genome-wide survey to interrogate the miRNA expression repertories in the hippocampus and spinal cord from an FUS mouse model. In this model, the transgenic FUS gene mimics the endogenous expression level and pattern within the central nervous system (CNS).[42] In the present study, we found that increasing FUS expression elicits a differential neural response in the spinal cord and hippocampus. miRNA-seq revealed miRNA expression signatures that are intrinsic to different CNS regions and differentially expressed miRNAs due to the increased FUS level. A subset of commonly up-regulated miRNAs down-regulate their predicted targets more strongly in the spinal cords than hippocampus, suggesting distinct responses in the two tissues in response to the increased FUS level. Among them, miR-1197 targets *Trib2*, a pro-survival pseudokinase involved in cell proliferation and apoptosis; whereas miR-488 and miR-496 targets *Vapb* and *Mbnl1*, respectively, both of which have been implicated in ALS. Reduced *TRIB2* protein is found in the ALS patient iPSC-derived motor neurons. Direct *TRIB2* knockdown reduces the survival of iPSC-derived human motor neurons. Critically, pharmacological stabilization of TRIB2 protein by epidermal growth factor receptor (EGFR) family kinase inhibitors was able to rescue the decreased survival of ALS motor neurons. Thus, our data suggest that FUS-mediated miRNA dysfunctions contribute to motor neuron damage, and TRIB2-mediated apoptosis may be a convergent pathway for motor neuron death in ALS.

RESULTS

Spinal cord motor neurons and hippocampal neurons respond differentially to increased FUS levels

One of the key questions in the major neurodegenerative diseases is why particular neuronal populations selectively degenerate in their respective diseases, such as motor neurons in ALS. We and others have previously shown that increased FUS level in the central nervous system (CNS) is sufficient to trigger motor dysfunctions and motor neuron degeneration in mice.[41,42] To investigate whether this is a region-specific effect, we made use of this FUS model mouse[42] by focusing on two distinct CNS regions: the spinal cord and hippocampus. Total homogenates from both the spinal cord and hippocampus prepared from animals with the three genotypes (non-transgenic, heterozygous, and homozygous for the FUS transgene insertion) were used for immunoblotting. In these mice, the human wild type FUS transgene expression was driven by the murine prion promoter and hereafter referred as het-hFUS^{WT}, or homo-hFUS^{WT}, respectively. Using an antibody that was previously validated to have an equal affinity to human and mouse FUS,[26,42] we detected a dose-dependent down-regulation of endogenous FUS as expression of human transgene increases (Figure 1A). Dose-dependent down-regulation of mouse FUS at the mRNA level was verified by qRT-PCR assay (Figure S1A), further confirming the presence of the autoregulatory mechanism for FUS expression[26,42,54,55] in both the spinal cord and hippocampus. The motor neurons in the homo-hFUS^{WT} mice showed p62/sequestosome accumulations, a sign of increased autophagy, without apparent FUS aggregates (upper panel of Figure 1B).[42] By contrast, immunofluorescence staining of hippocampal neurons showed normal nuclear localization of FUS and no apparent p62 accumulation in het-hFUS^{WT} and homo-hFUS^{WT} mice (lower panel of Figure 1B).

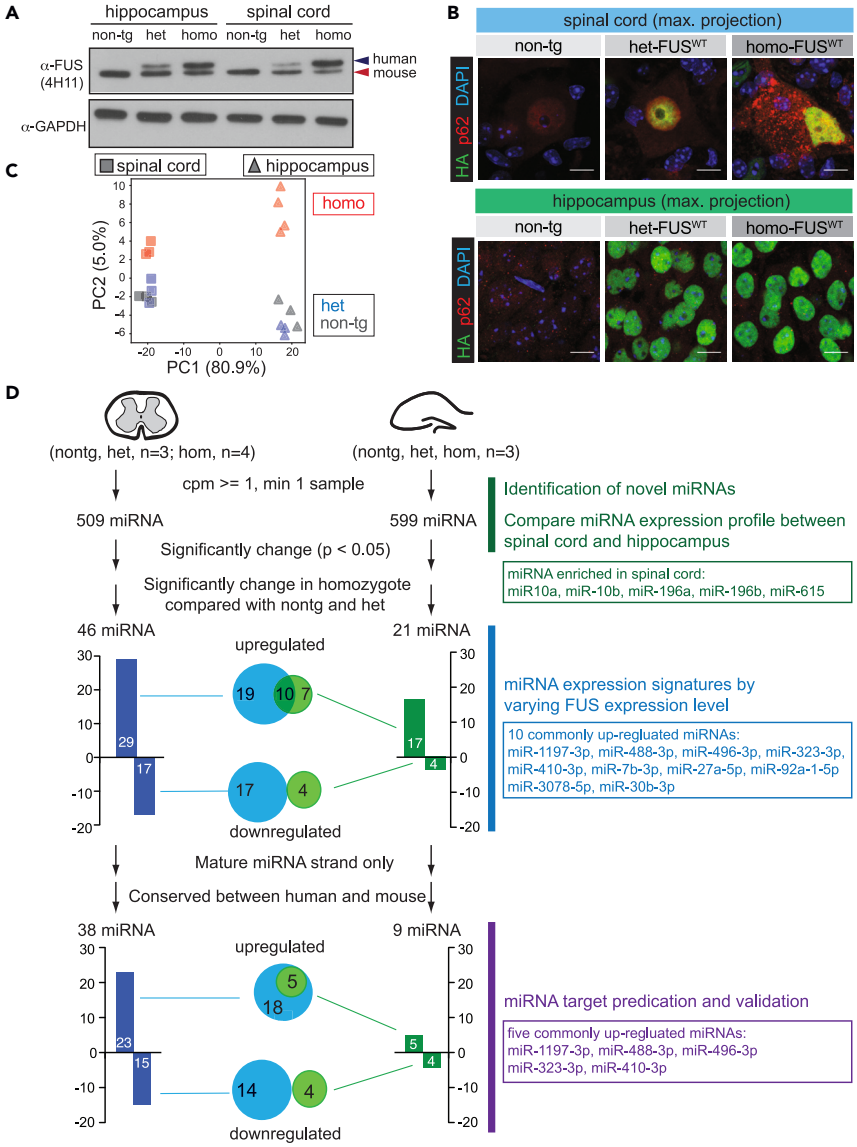

Figure 1. miRNA profiling in the spinal cord and hippocampus of an FUS mouse model

(A) Immunoblot analyses of human wild-type FUS transgene and mouse endogenous FUS from the hippocampi and spinal cords. Expression levels of FUS were evaluated using an antibody with comparable affinity to both human and mouse FUS. Upper (blue arrow) and lower (red arrow) bands are human and mouse FUS, respectively. Increased FUS level leads to a dose-dependent down-regulation of endogenous FUS in both the hippocampi and spinal cords.

(B) Immunofluorescent image of a spinal cord motor neuron (upper panel) and hippocampal CA3 pyramidal neurons (lower panel) co-labeled with HA (for the human FUS transgene) and p62/SQSTM1, an autophagy marker. p62 aggregates were readily observed in motor neuron from the homozygous FUS mouse (homo-FUS^{WT} mice), but not in the other genotypes (non-transgenics, or het-FUS^{WT} mice). By contrast, there were no p62 aggregates in the pyramidal neurons across all three genotypes (non-transgenics, het-FUS^{WT} mice, or homo-FUS^{WT}). Different CNS regions respond differentially to increasing FUS level. Scale bar, 10 μm.

(C) Principal component analysis (PCA) of miRNA expression data from the hippocampi and spinal cords of an FUS mouse model. The percentages in the axis labels indicate the percentages of explained variances. miRNA expression successfully segregates samples from the two CNS regions. Homo-FUS^{WT} mice segregate from the two genotypes (non-transgenics, and het-FUS^{WT} mice).

(D) Schematic flow chart of miRNA expression analysis in the spinal cords and hippocampi.

Differential miRNA expression patterns in the spinal cord and hippocampus

To understand how FUS-mediated miRNA dysfunction may lead to neuronal dysfunction and/or neurodegeneration, we systematically profiled miRNA expression in the spinal cords and hippocampi from this FUS mouse model (Figures 1C and 1D). Total RNA was extracted from dissected tissues and small RNA libraries were constructed for Illumina sequencing. Each of the libraries yielded ~7 to 16 million 18-to-30 nt

reads that could be perfectly mapped to the mouse genome sequence, with ~82.52%–96.72% of reads mapping to annotated miRNA hairpins[56] (Table S1).

To first test whether there are miRNA expression signatures that distinguish the two CNS regions (spinal cord vs. hippocampus) and the disease states (homo-hFUS^{WT} vs. non-transgenics and het-hFUS^{WT}), we performed principal component analysis (PCA) using miRNA genes that were expressed at ≥1 cpm (counts per million) at least in one library. The miRNA profiles clearly separated samples from the two tissues as well as their disease states (Figure 1C). Encouraged by the results, we next aimed to determine whether underlying molecular mechanisms for FUS-mediated neuronal dysfunctions and degeneration could be revealed by the miRNA profiling data.

To systematically analyze FUS-mediated miRNA changes (Figure 1D), we first determined the miRNA expression repertoires in the spinal cords and hippocampi of non-transgenic animals. We found 186 up-regulated and 173 down-regulated miRNAs in spinal cord when compared to the hippocampus ($p < 0.05$, FDR (BH) adjusted p value) (Table S2). Among these miRNAs, there were fifty-seven miRNA species that were overall enriched by at least 4-fold in the spinal cord compared to the hippocampus (Figure S2A; and Table S2). Five of these spinal cord enriched miRNA genes (miR-10a, miR-10b, miR-196a, miR-196b, miR-615) are embedded in the HOX gene clusters, and their expressions are restricted to the posterior part of the central nervous system, i.e., the spinal cord.[57–59] This suggested that the most prominent difference in the miRNA expression profile between the hippocampus and spinal cord is derived from the spatial information of their developmental origins.

Since miRNA annotation has not been comprehensively analyzed in these tissues, we predicted that there could be novel miRNA genes in our deeply sequenced library set, which contained >208 million mappable reads from each tissue (Table S1). To perform comprehensive miRNA expression profiling, we first sought to identify novel miRNA genes using our dataset. Using the mirdeep2 pipeline,[60] candidate miRNA loci were identified by requiring stringent evidence for processing by specific processing machineries (see miRNA-seq library preparation and sequencing, and bioinformatics analysis) similar to our previous studies.[61,62] Six canonical miRNAs (including one antisense miRNA that is orthologous to rat *mir-3546*) and one mirtron passed our criteria (Figure S2B; Table S3). Canonical miRNA genes typically contained additional sequence motifs known to facilitate recognition by the microprocessor complex.[63,64] The presence of the motifs in many of the novel miRNAs further demonstrates that they are genuine miRNA genes (Figures S2C, S2D, and S3; Table S3). The mirtron was found in an intron of the *KIF5C* host gene, which is specifically expressed in the nervous system (Figure S2D; Table S3). Collectively, the two sets of small RNA libraries allowed us to comprehensively understand the miRNA expression profiles in both the hippocampus and the spinal cord with an unprecedented sensitivity.

Elevating FUS levels results in distinct yet overlapping miRNA signatures in spinal cord and hippocampus

Our small RNA library analysis faithfully reported relative miRNA expression levels in the two tissues as well as different genotypes (Figures 1C and 1D). This result was consistent with the phenotypic analysis, where no obvious symptoms were observed in heterozygous transgenic animals at this age point,[42] as well as the total FUS protein level that was largely unchanged in the heterozygous transgenics in both the spinal cord and hippocampus (Figure 1A). There is an apparent trend where PC1 separates the tissue while PC2 does it based on the genotype, suggesting that there is a distinct miRNA expression signature characteristic to the homozygous animals mostly commonly seen in the spinal cord and the hippocampus.

We next compared the miRNA expression levels between homo-hFUS^{WT} homozygous transgenic animals and the controls (hereafter, we refer to non-transgenic and het-hFUS^{WT} animals as "controls"). fortysix and 21 miRNAs showed significant differences in the normalized expression levels in both comparisons (homo-hFUS^{WT} vs. non-transgenics and homo-hFUS^{WT} vs. het-hFUS^{WT}) in the spinal cord and the hippocampus, respectively (Figures 1D, 2A, and 2B; Tables S4 and S5, $p < 0.05$, FDR (BH) adjusted p value). Among the 46 significantly changing genes in the spinal cord, 29 and 17 genes were up- and down-regulated, while 17 and 4 genes were up- and down-regulated in the hippocampus, respectively (Figure 1D; Tables S4 and S5). The fact that larger numbers of genes were up-regulated in both tissues was consistent with the proposed function of FUS in promoting processing of a subset of miRNAs.[31] When the fold-change values were plotted against their average expression levels, differentially expressed genes were distributed in a wide range of expression levels. Thus, this excluded the possibility that the observed differential levels were mere artifacts stemming from the higher fluctuation of expression values for lowly expressed genes (Figures 2A and 2B). Furthermore, the library data were highly reproducible in the replicates, indicating that our small RNA data provide reliable information to differentiate miRNA expression patterns (Figures 2C and 2D).

Next, we determined whether miRNA expression changes were generally common or distinct between the two tissues. We found that 10 miRNA genes were commonly up-regulated in the spinal cord and the hippocampus, without any commonly down-regulated gene between them (Figures 1D and 2E). Four of these commonly up-regulated miRNAs (miR-1197-3p, miR-323-3p, miR-410-3p, and miR-496-3p) were derived from miR379-410 cluster within the imprinted *Dlk1-Dio3* loci.[65,66] This overlap suggests that the list of commonly up-regulated genes might contain core FUS target miRNAs underlying the FUS-transgene phenotypes.

To independently verify the small RNA-seq results, we performed qRT-PCR on selected miRNAs by focusing on genes belonging to the following five categories: miRNAs that are (i) commonly up-regulated in both the spinal cord and hippocampus (e.g., miR-1197-3p, miR-323-3p, and miR-488-3p), (ii) up-regulated specifically in spinal cord (e.g., miR-21a-5p, and miR-203-3p), (iii) up-regulated specifically in hippocampus (e.g., miR-488-5p), (iv) down-regulated specifically in spinal cord (e.g., miR-484), and (v) up-regulated in spinal cord but down-regulated in hippocampus (e.g., miR-146-5p) (Figure S4A). Data from qRT-PCR of these miRNAs not only corroborated with the changes observed in small RNA-seq data, they were also quantitatively comparable (Figure S4B). Collectively, these data indicated that increased FUS levels lead to distinct and overlapping miRNA signatures in both the spinal cord and hippocampus.

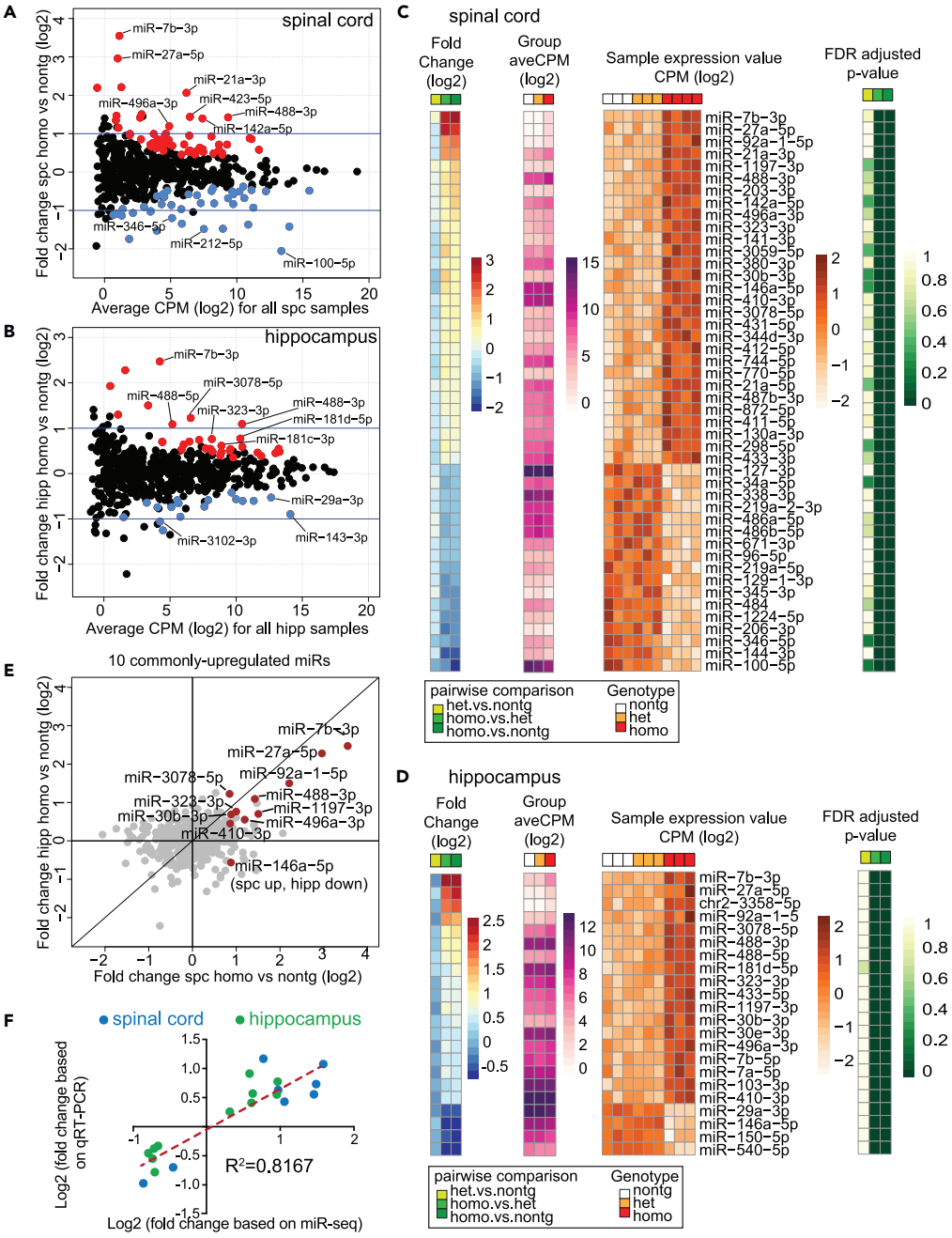

Figure 2. Varying FUS levels affects miRNA expression in the spinal cords and hippocampi

(A and B) Comparison of miRNA expression between non-transgenic and FUS model animals in the spinal cord (A) and hippocampus (B). Fold change values were calculated by dividing the average of normalized miRNA expression values of FUS model mice by those of non-transgenic mice. miRNA genes that are significantly highly or lowly expressed in FUS model animals ($p < 0.05$, FDR (BH) adjusted p value) are colored with red or blue, respectively.

(C and D) Summary of miRNA profiling in FUS model and non-transgenic mice in the spinal cord (C) and the hippocampus (D). Only significantly differentially expressed miRNA genes were used. The heatmaps show log2 of fold change values (the model mouse value divided by the non-transgenic value), log2 of average CPM values of the replicates in each group, row-normalized z-scores of all replicates and p values (FDR (BH) adjusted p value) between the indicated comparisons are shown. For comparisons between groups, see the legend for the comparison color coding.

(E) Comparison of fold change values between the spinal cord (X axis) and the hippocampus (Y axis). Log2 of fold-change values (The FUS model value divided by the non-transgenic value) are plotted. Commonly de-regulated miRNAs due to increased FUS level in the spinal cords and hippocampus are colored with red. These include 10 commonly up-regulated miRNAs and one oppositely regulated miRNA.

(F) Co-relation between miRNA-seq reads and qRT-PCR assays. Y- and X-axis are the log2 (fold change) based on qRT-PCR assays and miR-seq reads, respectively. Each dot represents an individual miRNA. The data from spinal cord and hippocampus are color-coded with blue and green, respectively.

Tissue-specific mRNA targets of the commonly up-regulated miRNAs

To further determine whether these deregulated miRNAs due to the increased FUS level have any biological consequences, we focused our analyses on the mature miRNAs that were conserved between mouse and human. Using these criteria, we identified 38 (23 up-regulated, 15 down-regulated) and nine (five up-regulated, four down-regulated) miRNAs that were significantly altered in the spinal cord and hippocampus, respectively. Intriguingly, the remaining five mis-regulated miRNAs (miR-1197-3p, miR-488-3p, miR-496-3p, miR-323-3p, and miR-410-3p) in the hippocampi were also up-regulated in the spinal cords and homo-hFUS^{WT} mice, whereas no commonly down-regulated miRNAs were found. We further characterized the five miRNAs that were up-regulated in both the spinal cord and hippocampus and identified the potential mRNA targets for these upregulated miRNAs (Figure 3). Using TargetScan[67] and RNA-seq data,[42] we prioritized the targets within the conserved seed regions across multiple species, in particular between human and mice. To experimentally validate that the putative mRNAs are bona fide miRNA targets, we performed luciferase-based report assays. Specifically, 3′-UTRs containing the seed target sites of the commonly misregulated miRNA genes were subcloned into the 3′-UTR after the coding region of *Renilla* luciferase in a dual luciferase reporter plasmid. This plasmid also contains a firefly luciferase as a control for transfection and expression. To confirm that the regulation by miRNAs was through the predicted target sites, the seed target sites were mutated at positions 3, 4, and 6. For the mRNA targets with multiple seed sites, the seed sites were either mutated individually or in combination. We used either miRNA mimic control or miR-mimics and the ratio of *Renilla* luciferase to firefly luciferase was used to measure the inhibitory effect of miRNA (Figures 3B and S5–S7). The predicted target 3′UTRs for the five commonly up-regulated miRNAs showed clear derepression of the mutated sensor in the presence of the corresponding miRNA mimics, validating functional miRNA-target relationships for the eight mRNA targets: *Trib2* for miR-1197-3p, *Mbnl1* and *Cyp26b1* for miR-496-3p, *Vapb* for miR-488-3p, *Klf11* and *Ubap2* for miR-323-3p, *Slc25a42* for miR-410-3p (Figures 3B and S5A).

We next determined whether these putative mRNA targets were down-regulated in the spinal cord and hippocampus of the FUS mouse models by qRT-PCR. All seven mRNA targets were down-regulated in the spinal cord of the homo-hFUS^{WT} mice (Figures 3C and S5B). Among these, *Vapb* and *Ubap2* were also down-regulated in the hippocampi of the homo-hFUS^{WT} mice (Figures 3C and S5B). Compared with the hippocampi, these five commonly up-regulated miRNAs showed higher fold-change values in the spinal cords (Figure 3D, column "Log_2 [Fold Change]"). Furthermore, only one of the five miRNAs (miR-488-3p) had a higher expression in the spinal cord (Figure 3D, column "Expression [cpm]"). This suggests that differential responses of target mRNAs may be due to the intrinsic difference of CNS regions, i.e., spinal cord versus hippocampus, or threshold effect of miRNA-mRNA interaction, i.e., higher miRNA increase needed to elicit a target downregulation. Nevertheless, the data were consistent with the notion that mis-regulation of specific miRNAs contributed to the changes in the miRNA profile caused by the elevated FUS level.

Reduced Trib2 expression in the spinal cord of ALS-FUS model and ALS patient iPSC-derived motor neurons

We identified *Trib2* as a target of miR-1197-3p (Figure 3B). TRIB2 is a pseudokinase that acts as a scaffold protein for E3 ubiquitin ligase and its expression is linked with cell proliferation and cell death.[68] Decreased TRIB2 levels lead to apoptosis,[69] whereas increased TRIB2 promotes cell growth and proliferation.[70,71] After validating the specificity of TRIB2 antibody and confirming that over-expressing miR-1197 reduces TRIB2 protein (Figure S8), we confirmed that TRIB2 protein level was reduced in the spinal cord, but not the hippocampus of the homo-hFUS^{WT} mice, whereas the TRIB2 protein remained comparable between non-transgenic and het-hFUS^{WT} mice (Figures 4A and 4B), which is consistent with the qRT-PCR results (Figure 3C).

Because of Trib2's role in proliferation and apoptosis,[69] we hypothesized that Trib2 dysregulation may contribute to motor neuron dysfunction and death. To this end, we investigated whether Trib2 deregulation could be detected in the ALS patients with FUS mutations. In the postmortem healthy control, FUS and TRIB2 are located predominantly in the nucleus of motor neurons in the lumbar enlargement of the spinal cord (upper panel in Figure 4C). In contrast, motor neurons from lumbar spinal cord of an ALS patient carrying an FUS(G504Wfs*12) mutation showed reduced nuclear TRIB2 staining as the deletion of two nucleotides at the exon 14 of FUS causes a frameshift that disrupts the nuclear localization signals (Figure 4C).[72,73] In addition, both TRIB2 and FUS colocalize and form aggregates in cytosol (lower panel of Figure 4C). Taken together, TRIB2 perturbance can be validated in patient motor neurons with known pathogenic FUS mutation and their interaction in cytoplasmic aggregates.

Next, we examined postmortem cervical and lumbar spinal cords from controls and sporadic ALS (sALS) patients. Cervical and/or lumbar sections of 10 controls and 10 sALS patients were stained for TRIB2 (Figures 5A and 5B), and the expression levels were measured to compare their levels within the motor neurons. While statistically not significant, TRIB2 expression was apparently decreased in the majority of motor neurons of ALS patients (box and whiskers plots and scatterplot, Figure 5C), averaging signals according to each human subject revealed a mean difference between control and sALS is −0.0296 [95.0%CI -0.0749, 0.0207] with the p value of the two-sided unpaired t test of 0.1228 (estimation plot, Figure 5C).

To better quantitatively assess TRIB2 level and independently verify whether TRIB2 is down-regulated in ALS motor neurons, we performed TRIB2 RT-qPCR in motor neurons derived from control and familial (including SOD1^{L144F}, TDP-43^{G298S}, and C9ORF72 expansion) and sALS patients (Figure 5D). TRIB2 mRNA is significantly reduced to 45–84% of control level ($p < 0.01$) in motor neurons derived from all 3 familial ALS and 2 sALS (Figure 5D), suggesting reduced TRIB2 level may be a common feature for ALS motor neurons.

Pharmacological stabilization of TRIB2 protein restores motor neuron survival in sporadic ALS motor neurons

To directly test whether TRIB2 reduction could lead to a reduction in neuronal survival, we knocked down TRIB2 in human iPSC-derived motor neurons (Figure 6A). Downregulation of TRIB2 by siRNA reduced its mRNA level to 27% ($p < 0.01$) (Figures 6B–6I) and caused ~24% reduction

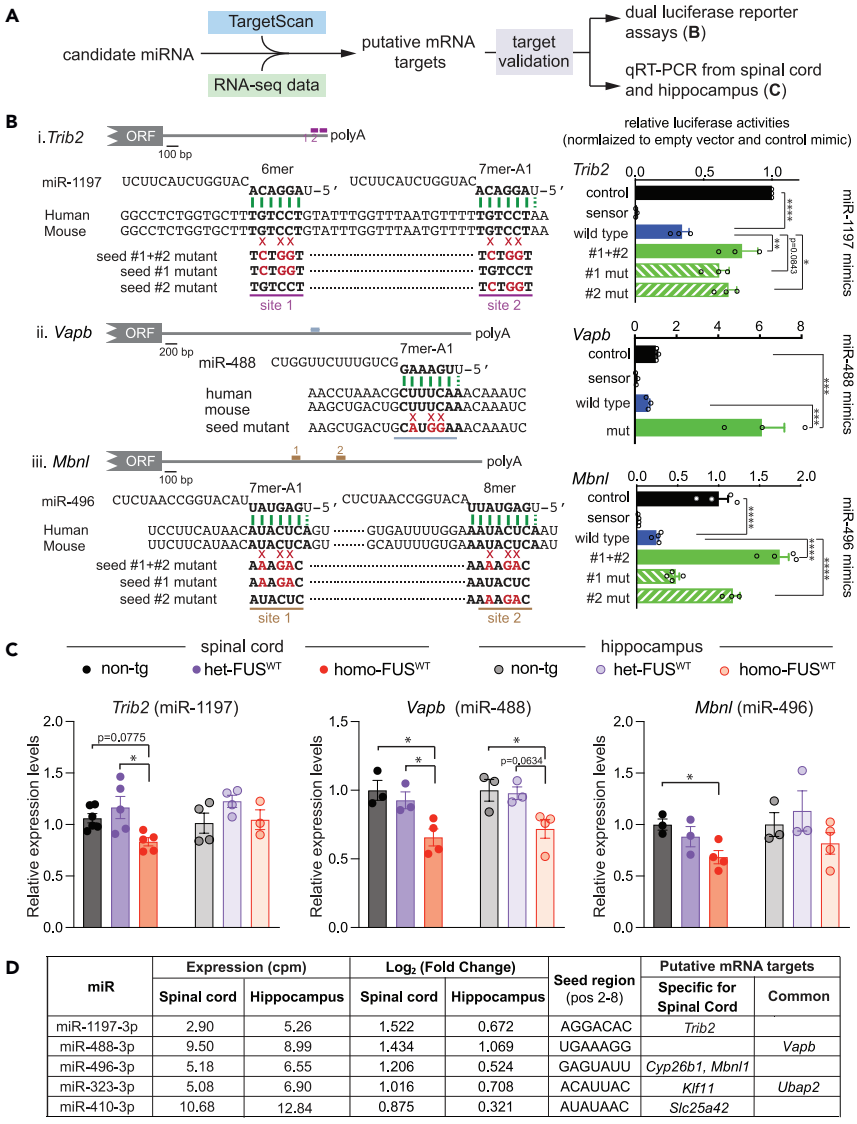

D

miR	Expression (cpm)		Log$_2$ (Fold Change)		Seed region (pos 2-8)	Putative mRNA targets	
	Spinal cord	Hippocampus	Spinal cord	Hippocampus		Specific for Spinal Cord	Common
miR-1197-3p	2.90	5.26	1.522	0.672	AGGACAC	*Trib2*	
miR-488-3p	9.50	8.99	1.434	1.069	UGAAAGG		*Vapb*
miR-496-3p	5.18	6.55	1.206	0.524	GAGUAUU	*Cyp26b1, Mbnl1*	
miR-323-3p	5.08	6.90	1.016	0.708	ACAUUAC	*Klf11*	*Ubap2*
miR-410-3p	10.68	12.84	0.875	0.321	AUAUAAC	*Slc25a42*	

Figure 3. Identification and validation of miRNA-mRNA targets for the commonly up-regulated miRNAs in the spinal cords and hippocampi

(A) Schematic for identification and validation of miRNA-mRNA target pairs. Dual luciferase assay was performed to determine the effect of putative miRNA seed target sequences. psiCHECK reporter has two luciferases, each is driven by its own promoter. The putative miRNA target sequence can be inserted into the 3-UTR of the *Renilla* luciferase, whereas the firefly luciferase is used for normalization. The luciferase reporter was co-transfected with either miR control mimic or miR mimics.

(B) Sequences (left) and results from the luciferase assays (right). Individual miRNA sequence with the seed sequence (bold) were aligned with putative human and mouse mRNA targets. The target sequences were shown in bold font. Positions 3, 4, and 6 of putative miRNA target sequences were mutated (red). When more than one seed target was identified, the predicted seed target regions were mutated individually and in combination (e.g., #1 mutant, #2 mutant, and #1+#2 mutant). The ratio of the readings of *Renilla* luciferease and firefly luciferase was first calculated for each combination of the reporter and the mimic, and subsequently the ratios were normalized with that of the miR mimic control with the same sensor plasmid. How the assays were normalized can be found in Figures S6 and S7. Ordinary one-way ANOVA with Tukey's multiple comparison correction is used. *, $p < 0.05$; **, $p < 0.01$; ***, $p < 0.001$; ****, $p < 0.0001$. For simplicity, not all statistic results were given.

(C) RT-qPCR for putative mRNA targets in the spinal cords and hippocampi of non-transgenics, het-FUS^{WT}, and homo-FUS^{WT}. At least 3 independent biological samples (indicated by each dot) were used per qRT-PCR assay, Ordinary one-way ANOVA with Tukey's multiple comparison correction is used. *, $p < 0.05$; **, $p < 0.01$; ***, $p < 0.001$. Solid bars and bars with diagonal lines show relative expression levels compared to the non-tg control in spinal cords and hippocampi, respectively.

(D) Summary of five commonly up-regulated miRNAs, their expression changes in spinal cords and hippocampi resulting from increased FUS level, and their putative mRNA targets.

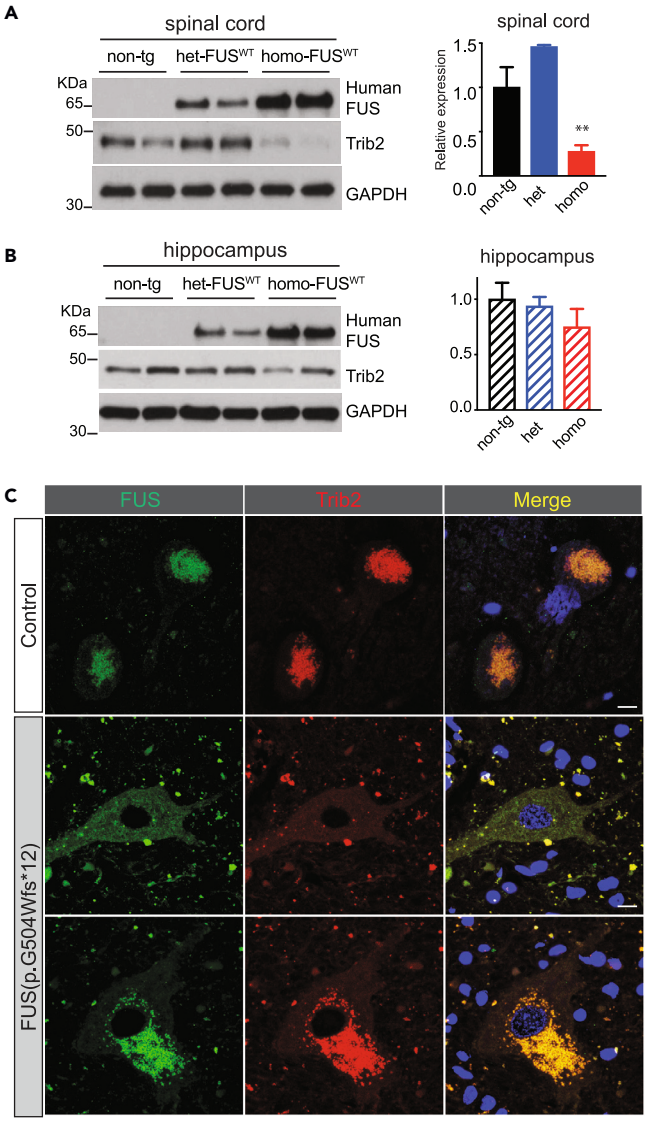

Figure 4. TRIB2 as a potential target caused by FUS dysfunction

(A and B) Immunoblot analyses of TRIB2 in the spinal cords (A) and hippocampi (B) of an ALS-FUS mouse model. Expression of FUS transgene was confirmed using anti-HA antibody. The charts show the quantified results. Increased FUS level down-regulates TRIB2 in the spinal cords, but not the hippocampus.

(C) Immunofluorescence images of lumbar spinal cords of a healthy control and an ALS-FUS patient (FUS(p.G504Wfs*12) co-labeled with FUS (green), Trib2 (red), and DAPI (blue). Both FUS and Trib2 show nuclear immunoreactivity in the motor neurons of a healthy control (upper panel). In contrast, FUS and Trib2 are depleted in the nucleus, but they are localized in the cytoplasm or cytoplasmic inclusions in patient motor neurons. Scale bar, 10 μm.

($p < 0.05$) of Islet-positive motor neurons (Figures 6B–6ii). Furthermore, activated caspase-3, a marker for apoptosis, was significantly higher (20% increase, $p < 0.05$) in the motor neurons treated with Trib2 siRNA (Figure S9). Similarly, over-expressing miR-1197 in human iPSC-derived motor neurons reduced *TRIB2* mRNA and protein expression (Figures 6C–6I-ii). Compared with the control, miR-1197 mimic reduced the Islet1-positive motor neurons by ~20% (Figures 6C–6iii). Taken together, the data suggest that reduced TRIB2 expression is sufficient to trigger motor neuron death.

To probe the potential of targeting TRIB2 for therapy, we took advantage of previous work by Foulke and colleagues, where they explore the available Published Kinase Inhibitor Set (PKIS) for small molecules that either destabilize or stabilize TRIB2 protein.[70] TAK-285 and lapatinib, the latter of which is used to treat breast cancer and other solid tumors under the trade name Tykerb, were shown to stabilize TRIB2 protein.[70] We reasoned that if TRIB2 protein could be stabilized by these small molecules at the post-translational level, one should be able to rescue TRIB2-mediated cell death. To this end, we lowered TRIB2 level in human motor neurons by over-expressing miR-1197 mimics (Figures 7A and 7B). While treatment of TAK-285 and lapatinib did not increase TRIB2 mRNA level as expected (Figure 7A), TRIB2 protein

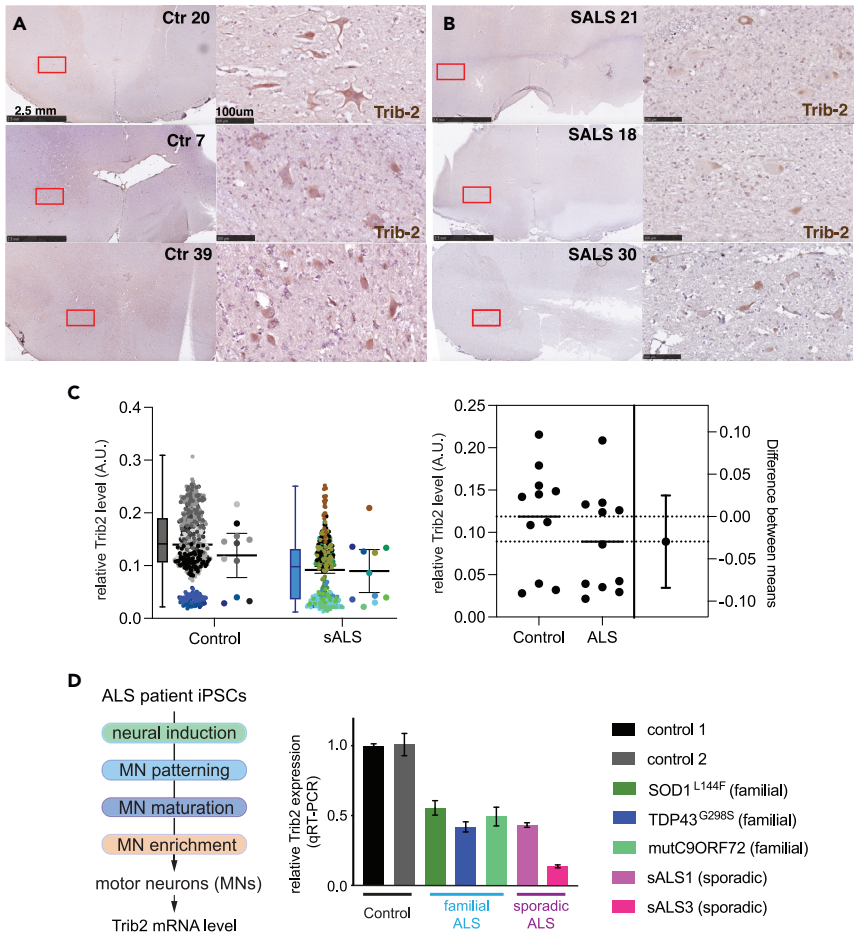

Figure 5. Reduced TRIB2 expression in ALS patient-derived motor neurons

(A) TRIB2 expression levels in cervical sections of controls patients. Left column is the view map of the tissue. Red square is magnified in the right panel of each section.

(B) Trib2 expression in sALS patients. Left panels are the map view of the tissue and the red square is magnified in the right panels. Levels of expression of TRIB2 = were downregulated in sALS patients motor neurons compared with controls.

(C) Comparison of TRIB2 expression levels in each motor neuron. Scatterplot was used to represent all analyzed motor neurons (control: 552 motor neurons from cervical and/or lumbar of 10 control subjects; sALS: 304 motor neurons from 10 sALS patients). Color coded dots indicate motor neurons from the specific human subject. The average TRIB2 signal was calculated and plotted as a single datapoint on the right. Error bar represents 95% CI. The mean difference between control and sALS is shown in the Gardner-Altman estimation plot on the right. Both groups are plotted on the left axes; the mean difference is plotted on the right axes. The mean difference between control and sporadic ALS is −0.0296 [95.0%CI -0.0749, 0.0207] with the p value of the two-sided unpaired t-test of 0.1228.

(D) TRIB2 mRNA level in motor neurons derived from control and human ALS patients. Left panel: schematic of motor neuron differentiation and enriched from human iPSCs. Middle panel: TRIB2 RT-qPCR.

levels were restored to near control treatment (i.e., miR-mimic control) (Figure 7B). Critically, TAK-285 and lapatinib treated motor neurons showed similar survival as control (Figure 7C). Because the original intended targets for TAK-285 and lapatinib are EGFR, we examined whether the beneficial effects could also be due to alternation in EGFR signaling. As activation of EGFR leads to increased phosphorylation of AKT at Thr308 residue, we quantified phospho-Thr308 (T308) of AKT and total AKT level using immunoblot. No significant changes in phospho-T308 and AKT were observed with TAK-285 and lapatinib treatment (Figure S10). Thus, the data suggest that restoration of TRIB2 protein expression could extend motor neuron survivals.

To further test whether reduced TRIB2 expression correlates with reduced motor neuron survival and whether restoration of TRIB2 expression could extend motor neuron survival in a disease setting, we took advantage of the accelerated motor neuron degeneration in our iPSC-derived motor neuron model.[74] In this model, there is a ~20% reduction of motor neurons in sALS cultures between days 28 and 31, whereas there is no such reduction in survival using control motor neurons derived from non-diseased individuals.[74] Under this condition, the TRIB2 mRNA and protein levels showed a 26% ($p < 0.01$) and 29% reduction ($p < 0.05$), respectively, in motor neurons derived from a sALS patient at day 31 when compared with day 28 (Figures 7D and 7E). The reduced TRIB2 expression correlates with the reduced survival (23%, $p < 0.01$)

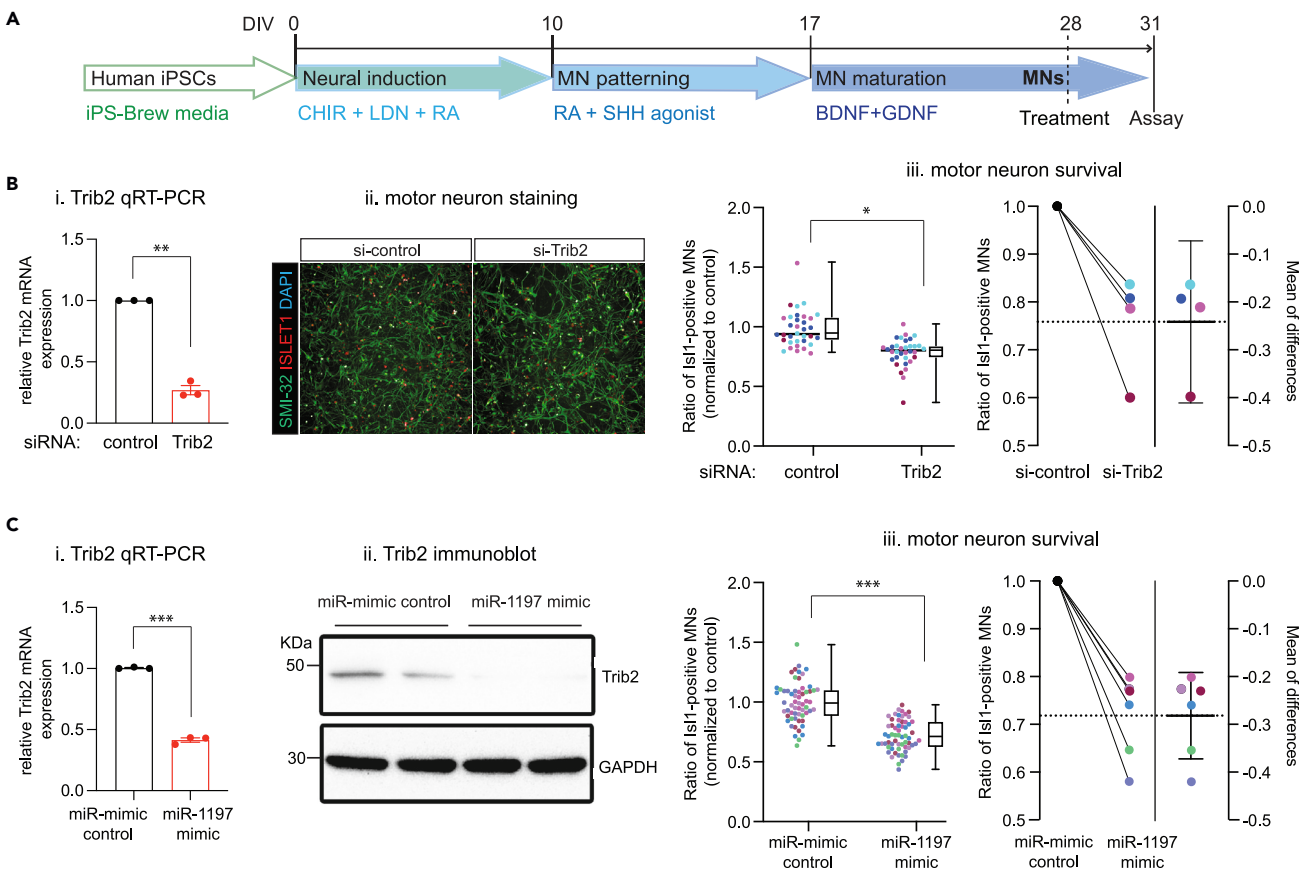

Figure 6. TRIB2 down-regulation and miR-1197 over-expression triggers degeneration in human iPSCs-derived motor neurons

(A) Schematic of human iPSC differentiation toward motor neuron lineage and experimental design.

(B) Human motor neurons treated with control siRNA and siRNA against TRIB2. (Bi) TRIB2 mRNA level in human motor neurons treated with control siRNA and siRNA against TRIB2. N = 3 for each treatment with normalization to control siRNA condition. Significance was tested using paired t test; **, $p < 0.01$. (Bii) Immunofluorescence images of iPSC-derived motor neurons treated with control siRNA and siRNA against TRIB2. Cells were co-labeled with SMI-32 (green), Islet1 (red) and DAPI (blue). Scale bar, 50 μm. (Biii) Quantification of Islet1-positive motor neurons in iPSC-derived motor neurons treated with control siRNA or siRNA against TRIB2. 4 independent experiments were performed. Each set of experiment has at least 8–10 biological replicates. Individual dot represents each biological sample with different color indicates each set of independent experiment. Each set of experiment is normalized with control siRNA treatment. Left panel showed individual data points, whereas the right panel estimation plot showed average of each independent experiment pair. Significance was tested using paired t test; *, $p < 0.05$.

(C) Human motor neurons treated with control miRNA mimics or miR-1197 mimics.

(Ci) TRIB2 mRNA level in human motor neurons treated with control miRNA mimics or miR-1197 mimics. N = 3 for each treatment with normalization to control miR-mimics condition. Significance was tested using paired t test; ***, $p < 0.001$. (Cii) Immunoblotting of TRIB2 for iPSC-derived motor neurons treated with miR mimic controls or miR-1197 mimic. Trib2 protein is reduced in motor neurons treated with miR-1197. (Ciii) Quantification of Islet1-positive motor neurons in iPSC-derived motor neurons treated with control miRNA mimics or miR-1197 mimics. 6 independent experiments were performed. Each set of experiment has at least 8–10 biological replicates. Individual dot represents each biological sample with different color indicates each set of independent experiment. Each set of experiment is normalized with control miR-mimics. Left panel showed individual data points, whereas the right panel estimation plot showed average of each independent experiment pair. Significance was tested using paired t test; ***, $p < 0.001$.

(Figure 7F). Furthermore, treating motor neurons derived from a sALS patient with lapatinib and TAK-285 restored TRIB2 protein expression to a level similar to that at day 28 without altering its mRNA level (Figure 7E). More critically, lapatinib and TAK-285 treatment rescued the motor neuron survival to that of motor neurons at day 28 ($p < 0.05$, for lapatinib treatment; $p < 0.01$ for TAK-285 treatment) (Figure 7F). Taken together, our results indicate that TRIB2 reduction contributes to motor neuron death and restoration of TRIB2 may offer a potential therapeutic option for ALS.

DISCUSSION

In this study, we investigated how FUS dysfunctions trigger pathogenic cascade in ALS. We hypothesized that FUS could coordinate the pre-mRNA and miRNA biogenesis, and discoordination of the processes may contribute to neuronal dysfunction through mis-regulation of

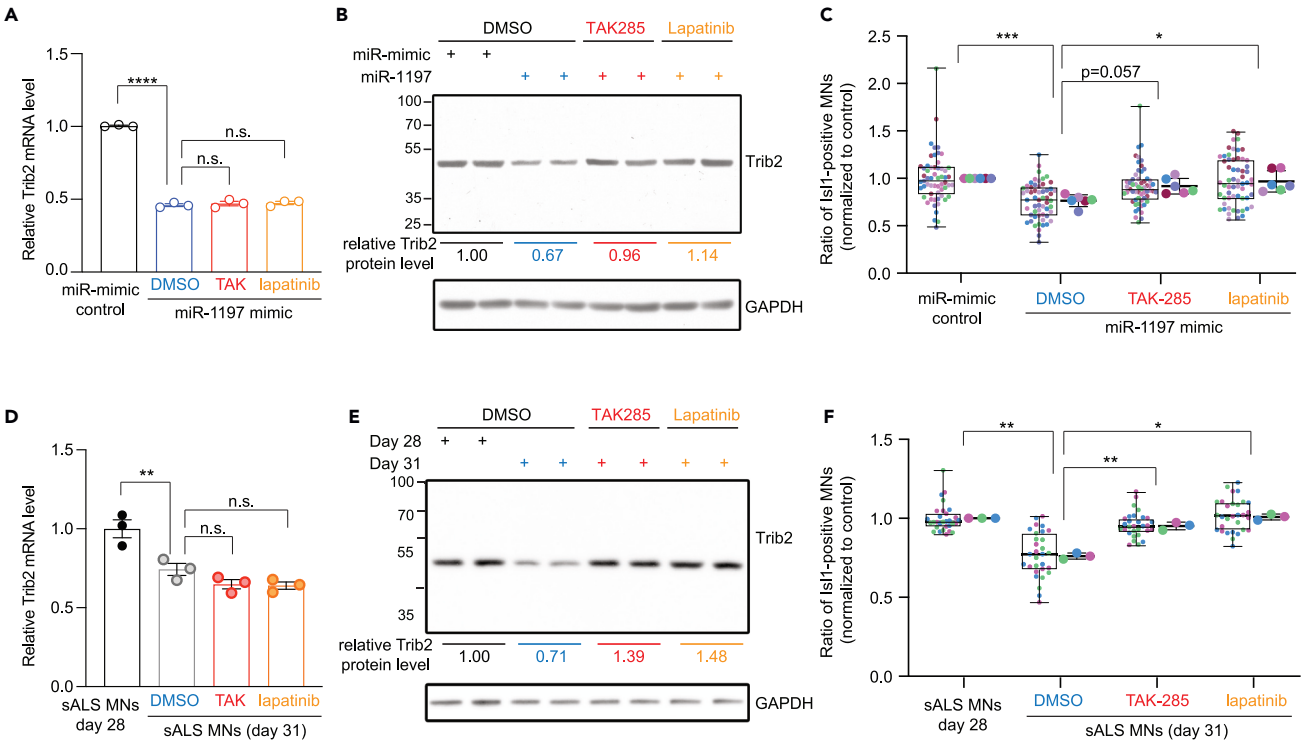

Figure 7. Stabilization of TRIB2 protein using EGFR kinase inhibitors rescue degeneration of iPSC-derived motor neurons treated with miR-1197 mimics and from a sporadic ALS patient

(A) TRIB2 mRNA level in human motor neurons treated with control miRNA mimics or miR-1197 mimics was assessed using RT-qPCR. DMSO was used to dissolve TAK-285 and lapatinib and added to control miR-mimics for control. Quantifications were done with three independent batch of treatments (n = 3). One-way ANOVA with Tukey's multiple comparisons tests was used to evaluate statistical significance, ****, $p < 0.0001$.

(B) Immunoblotting of TRIB2 in human motor neurons treated with control miRNA mimics or miR-1197 mimics. DMSO was used to dissolve TAK-285 and lapatinib and added to control miR-mimics for control. TRIB2 immunoreactivities were quantified and normalized to control miR-mimics. TRIB2 protein level in combined treatment of TAK-285 and lapatinib treatment and miR-1197 mimics is comparable with control miR-mimics.

(C) Quantification of Islet1-positive motor neurons in iPSC-derived motor neurons treated with control miRNA mimics or miR-1197 mimics with DMSO, TAK-285, or lapatinib. Six independent experiments were performed. Each set of experiment has at least 8–10 biological replicates. Individual dot represents each biological sample with different color indicates each set of independent experiment. Each set of experiment is normalized with control miR-mimics. Left side showed individual data points, whereas the right side showed average of each independent experiment pair. One-way ANOVA with Tukey's multiple comparisons tests was used to evaluate statistical significance, *: $p < 0.05$; ***: $p < 0.001$.

(D) TRIB2 mRNA level in motor neurons derived from a sALS patient treated with DMSO at day 28 (no apparent degeneration) and with DMSO, TAK-285, and lapatinib at day 31 (motor neuron degeneration was observed). TRIB2 mRNA showed a time-dependent decline between day 28 and day 31. TAK-285 and lapatinib treatment did not affect Trib2 mRNA level.

(E) Immunoblotting of TRIB2 in sALS motor neurons treated with DMSO at day 28, and with DMSO, TAK-285, and lapatinib at day 31. Trib2 immunoreactivities were quantified and normalized to motor neurons at day 28. Trib2 protein level in TAK-285 and lapatinib treatment is increased when compared with to motor neurons at day 28.

(F) Quantification of Islet1-positive motor neurons in sALS motor neurons treated treated with DMSO at day 28, and with DMSO, TAK-285, and lapatinib at day 31. three independent experiments were performed. Each set of experiment has at least 8–10 biological replicates. Individual dot represents each biological sample with different color indicates each set of independent experiment. Each set of experiment is normalized with motor neurons at day 28. Left side showed individual data points, whereas the right side showed average of each independent experiment pair. One-way ANOVA with Tukey's multiple comparisons tests was used to evaluate statistical significance, *: $p < 0.05$; **: $p < 0.01$.

miRNAs. By comparing the miRNA repertoires in the spinal cord and hippocampus from an FUS mouse model expressing varying FUS levels in the CNS,[42] we predicted and revealed an intrinsic miRNA expression signatures that are CNS region-specific. Furthermore, elevated FUS levels led to changes in miRNA expression, where they are predominantly up-regulated in both the spinal cords and hippocampi. Five of these commonly up-regulated miRNAs were further investigated for their mRNA targets. Among these, miR-1197 within the miR-379-410 cluster targets TRIB2, a pseudokinase that regulates proliferation and apoptosis. Up-regulation of miR-1197 down-regulates TRIB2 in the spinal cords, but not hippocampi, suggesting a tissue-specific response to miRNA changes. Reduced TRIB2 expression was found in iPSCs-derived motor neurons from ALS patients. Direct down-regulation of TRIB2 by siRNA induces degeneration in human iPSC-derived motor neurons. Conversely, pharmacological stabilization of TRIB2 protein by two small molecules, one of which is a clinically

approved EGFR family kinase inhibitor, was able to rescue the survival of sALS motor neurons. Taken together, our data indicate that FUS-mediated miRNA dysfunctions selectively trigger motor neuron damage and Trib2-mediated cell death may be a convergent pathway for motor neuron death in ALS.

miRNA expression is regulated at multiple steps including transcriptional and post-transcriptional levels, and RNA-binding proteins (RBPs) play roles in regulating miRNA biogenesis.[75] The importance of the multi-layered regulation was further demonstrated by the genome-wide identification of the biochemical and functional interactions between RBPs and miRNAs.[76,77] Since (i) FUS has repeatedly been identified as an RBP that selectively binds subsets of miRNA transcripts in unbiased screens,[31,77] and (ii) elevated FUS expression preferentially upregulate miRNA levels, the data support our hypothesis that FUS regulates miRNA biogenesis. Four (miR-1197, miR-323, miR-410, and miR-496) out of these 10 commonly up-regulated miRNAs were located within the imprinting miR-379-410 cluster. The miR-379-410 cluster has been shown to regulate neuronal and dendritic morphogenesis,[78,79] and mice lacking the miR-379-410 locus showed enhanced anxiety.[80] Recently, long noncoding RNAs (lncRNAs) from *Dlk1-Dio3* region, which includes the miR379-410 cluster, is shown to be enriched in the motor neurons and is required to maintain motor neuron fates.[81] Together with our data, the imprinted *Dlk1-Dio3* regions that contains multiple classes of noncoding RNAs, including miRNAs,[65] may play an important role in normal and pathological CNS functions.

Reduced miRNA biogenesis has been reported to contribute to spinal muscular atrophy (SMA)-like phenotypes[82] and ALS.[83] Alternation of specific miRNAs, such as miR-218, miR-375, and miR-17∼92, contribute to motor neuron degeneration.[84–88] Our results that FUS-mediated miRNA deregulation contributed to triggering motor neuron death further underscore the importance of miRNA homeostasis in motor neurons. Our analysis also revealed that miR-488 and miR-496 targets *Vapb* and *Mbnl1*, respectively. Both *Vapb* and *Mbnl1* are implicated in ALS: mutations in *VAPB* have been identified for ALS[89]; whereas level of *Mbnl1* influences FUS-mediated toxicity.[90] In addition, studies using mouse ESC or human iPSC-derived motor neurons carrying ALS-linked mutations in FUS have also identified a numbers of mis-regulated miRNAs.[91,92] However, we note that different miRNAs were identified in these two studies and the mechanisms by which these deregulated miRNAs caused motor neuron dysfunctions appear to be distinct. In addition, we compared misregulated miRNAs in our FUS model and in previous studies using postmortem ALS patient samples studies.[83,87,93] While there are commonly misregulated genes showing changes in the same directions, the overlaps are rather small, and previously identified misregulated genes generally do not show similar trends (Figure S11). Therefore, the results did not allow us to make clear conclusions from our data with postmortem human tissue data. Nevertheless, expression of FUS itself is regulated through a regulatory feedback loop involving miRNAs and targets in the FUS 3′-UTR.[54] As a result, overexpression FUS without its 3′-UTR has been shown to cause ALS-like symptoms in mice.[42] Taken together, the results pointed to the possibility that one of the pathogenic mechanisms driving ALS is the complex regulatory network involving mutual regulation of the miRNA pathway and FUS expression.

Both the symptoms and pathology in familial and sporadic neurodegenerative diseases are indistinguishable. Genetic mutations identified in the familial form are typically implied as one of the underlying mechanisms for the sporadic form. Here, we identified TRIB2 as a miR-1197 target resulting from FUS dysfunctions. Increased FUS level appears to down-regulate and/or affect TRIB2 expression selectively in the spinal cords. TRIB2 knockdown causes apoptosis in T cell acute lymphoblastic leukemia cell lines[69] and knockdown of TRIB2 similarly caused cell death in iPSC-derived motor neurons. Although, we observed an apparent decreased TRIB2 expression in the spinal cord motor neurons from postmortem sALS patients, the results do not reach a statistical significance when averaging the TRIB2 levels according to each subject. It is plausible that the surviving motor neurons in ALS patients may have sufficient TRIB2 level to maintain their survival. For example, our previous work showed that the miR-218 reduction was only observed in ALS motor neurons bearing TDP-43 pathology, but not motor neurons with normal nuclear TDP-43 staining.[87] Nevertheless, reduced TRIB2 expression was observed in iPSC-derived motor neurons from ALS patients. Thus, the result is consistent with the notion that TRIB2-mediated cell death may be a common hallmark of ALS motor neurons. Apoptosis has been proposed as a potential mechanism for the premature death of ALS motor neurons.[94,95] Pharmacologically or genetically blocking apoptosis effectively preserved motor neuron functions and prolonged the life span of SOD1 mouse models, demonstrating the functional importance of apoptosis in the pathology.[96,97] In addition, inhibition of MAP4K4, which attenuates c-Jun-mediated apoptosis and activates autophagy, improved familial ALS motor neuron survival.[98] Thus, blocking apoptosis via multiple mechanisms may be more effective in rescuing motor neuron functions. The mechanisms by which TRIB2 exerts oncogenic and apoptotic abilities are under active investigation. The proposed mechanisms include modulating serine/threonine protein kinase AKT signaling,[71] and XIAP anti-apoptotic pathways.[69] In this study, we explored the potential therapeutic application by exploiting the pseudokinase domain of TRIB2 with the available PKIS, which was recently proposed by Foulke and colleagues for cancer treatment.[70] In particular, TAK-285 and lapatinib were able to restore TRIB2 protein and motor neuron survival. It is worth noting that lapatinib is an approved oral active drug for breast cancer and other solid tumors.[99] A similar approach may be utilized to identify potential compounds that modulate TRIB2 levels in motor neurons as potential therapeutic interventions.

Our strategy relying on miRNA expression profiles offers an efficient means to identify core regulatory networks underlying neurodegenerative diseases. Furthermore, the successful identification of TRIB2 as a key molecule that mediates cell death in motor neurons in patients raised the possibility that modulating the miRNA level could provide additional therapeutic interventions. Indeed, a similar strategy has recently been exploited to study FTD caused by a tau mutation in a mouse model to identify miR-203 as a key regulator in neurodegeneration. And the modulation of miR-203 activity was able to revert the disease-associated phenotype,[100] validating the value of such strategies in finding effective therapeutic options for neurodegenerative diseases.

Thus, our data suggest that (i) miRNA profiling may be utilized to investigate the molecular mechanisms underlying neurodegenerative diseases, and (ii) modulating TRIB2 level may provide an additional therapeutic intervention for ALS.

Limitations of the study

The miRNA profiling results in the present study may not necessarily reflect miRNA expression states in human patients especially those not caused by FUS abnormalities. Indeed, the mouse homologs of the miRNAs that were identified as up- or down-regulated genes in patients did not show consistent trends (Figure S11). The discrepancy may also stem from the difference in the disease stages at the time of sample collection.

STAR★METHODS

Detailed methods are provided in the online version of this paper and include the following:

- KEY RESOURCES TABLE
- RESOURCE AVAILABILITY
  - Lead contact
  - Material availability
  - Data and code availability
- EXPERIMENTAL MODEL AND STUDY PARTICIPANT DETAILS
  - Mouse models
  - Ethics approval and consent to participate
- METHOD DETAILS
  - RNA extraction and quantitative RT-PCR
  - miRNA-seq library preparation and sequencing, and bioinformatics analysis
  - Immunohistochemistry
  - Image acquisition
  - Immunoblotting
  - miRNA target prediction
  - Plasmid constructions
  - Cell culture, miR-mimic treatment, dual luciferase assay
  - Motor neuron differentiation from human induced pluripotent stem cells and enrichment
  - RNA interference and small molecule treatment in motor neuron cultures
  - Immunofluorescence, image acquisition and image analysis of iPSC-derived motor neurons
  - Immunohistochemistry, image acquisition and quantification, and immunoblotting using ALS patient tissues
- METHOD DETAILS: QUANTIFICATION AND STATISTICAL ANALYSIS

SUPPLEMENTAL INFORMATION

Supplemental information can be found online at https://doi.org/10.1016/j.isci.2023.108152.

ACKNOWLEDGMENTS

We thank both the Ling and Okamura laboratory members for their support, discussion, and suggestions. Graphic summary was generated using Biorender. This work was supported by grants to S.Ng and K.O from the National Research Foundation, Singapore, to S.H.K from National Research Foundation (NRF) funded by the Ministry of Science, Korea (NRF-2018M3C7A1056512), to S.-C.L from the Swee Liew-Wadsworth Endowment fund, National University of Singapore (NUS), National Medical Research Council (NMRC/OFIRG/0042/2017), Singapore, Ministry of Education (MOE-T2EP30220-0014), Singapore, and National Research Foundation (NRF-ISF003-3221), Singapore. S.-C.L dedicates this work to the loving memory of Sheue-Houy Tyan. We would also like to acknowledge the patients and families without which this research would not be possible.

AUTHOR CONTRIBUTIONS

Conceptualization, S.-C.L., K.O., W.Y.H., and F.L.; Methodology, W.Y.H., J.-H.H., F.L., S.D.-G., J.-C.C., E.S., M.J.R., D.A., S.M.L., Y.-L.C., Y.S., S.-Y.N., K.O., and S.-C.L.; Software, L.-L.C. and Y.S.; Validation, W.Y.H., J.-H.H., F.L., S.D.-G., J.-C.C., E.S., M.J.R., D.A., S.M.L., Y.-L.C, Y.S., S.-Y.N., K.O., and S-CL, Formal Analysis, W.Y.H., J.-H.H., F.L., S.D.-G., J.-C.C, E.S., M.J.R., D.A., S.M.L., Y.-L.C., Y.S., S.-Y.N., K.O., and S.-C.L.; Investigation, W.Y.H., J.-H.H., F.L., S.D.-G., J.-C.C., E.S., M.J.R., D.A., S.M.L., Y.-L.C., Y.S., A.X.S., S.-H.T., E.K., S.H.K., J.R., S.-Y.N., K.O., and S.-C.L.; Resources, A.X.S., S.-H.T., E.K., S.H.K., J.R., S.-Y.N., K.O., and S.-C.L.; Data Curation, W.Y.H., J.-H.H., F.L., S.D.-G., J.-C.C., E.S., M.J.R., D.A., S.M.L., Y.-L.C., Y.S., S.-Y.N., K.O., and S.-C.L.; Writing-Original Draft, S.-C.L., K.O., W.Y.H., L.-L.C., and F.L., Writing-Review & Editing, S.-C.L., K.O., and S.H.K., Visualization, W.Y.H., J.-H.H., F.L., S.D.-G., J.-C.C., E.S., M.J.R., D.A., S.M.L., Y.-L.C., Y.S., S.-Y.N., K.O., and S.-C.L.; Supervision, A.X.S., S.-H.T., E.K., S.H.K., J.R., S.-Y.N., K.O., and S.-C.L.; Project Administration, A.X.S., S.-H.T., E.K., S.H.K., J.R., S.-Y.N., K.O., and S.-C.L.; Funding Acquisition, E.K., S.H.K., J.R., S.-Y.N., K.O., and S.-C.L.

DECLARATION OF INTERESTS

The authors declare no competing interests.

INCLUSION AND DIVERSITY

We support inclusive, diverse, and equitable conduct of research.

Received: August 28, 2023
Revised: September 21, 2023
Accepted: October 3, 2023
Published: October 6, 2023

REFERENCES

1. Crozat, A., Aman, P., Mandahl, N., and Ron, D. (1993). Fusion of CHOP to a novel RNA-binding protein in human myxoid liposarcoma. Nature *363*, 640–644. https://doi.org/10.1038/363640a0.
2. Rabbitts, T.H., Forster, A., Larson, R., and Nathan, P. (1993). Fusion of the dominant negative transcription regulator CHOP with a novel gene FUS by translocation t(12;16) in malignant liposarcoma. Nat. Genet. *4*, 175–180. https://doi.org/10.1038/ng0693-175.
3. Ling, S.-C. (2018). Synaptic Paths to Neurodegeneration: The Emerging Role of TDP-43 and FUS in Synaptic Functions. Neural Plast. *2018*, 1–13. https://doi.org/10.1155/2018/8413496.
4. Lattante, S., Rouleau, G.A., and Kabashi, E. (2013). TARDBP and FUS Mutations Associated with Amyotrophic Lateral Sclerosis: Summary and Update. Hum. Mutat. *34*, 812–826. https://doi.org/10.1002/humu.22319.
5. Mackenzie, I.R., Rademakers, R., and Neumann, M. (2010). TDP-43 and FUS in amyotrophic lateral sclerosis and frontotemporal dementia. Lancet Neurol. *9*, 995–1007. https://doi.org/10.1016/S1474-4422(10)70195-2.
6. Tyzack, G.E., Luisier, R., Taha, D.M., Neeves, J., Modic, M., Mitchell, J.S., Meyer, I., Greensmith, L., Newcombe, J., Ule, J., et al. (2019). Widespread FUS mislocalization is a molecular hallmark of amyotrophic lateral sclerosis. Brain *142*, 2572–2580. https://doi.org/10.1093/brain/awz217.
7. Ling, S.-C., Polymenidou, M., and Cleveland, D.W. (2013). Converging Mechanisms in ALS and FTD: Disrupted RNA and Protein Homeostasis. Neuron *79*, 416–438. https://doi.org/10.1016/j.neuron.2013.07.033.
8. Robberecht, W., and Philips, T. (2013). The changing scene of amyotrophic lateral sclerosis. Nat. Rev. Neurosci. *14*, 248–264. https://doi.org/10.1038/nrn3430.
9. Gao, F.B., Almeida, S., and Lopez-Gonzalez, R. (2017). Dysregulated molecular pathways in amyotrophic lateral sclerosis–frontotemporal dementia spectrum disorder. EMBO J. *36*, 2931–2950. https://doi.org/10.15252/embj.201797568.
10. Kiernan, M.C., Vucic, S., Cheah, B.C., Turner, M.R., Eisen, A., Hardiman, O., Burrell, J.R., and Zoing, M.C. (2011). Amyotrophic lateral sclerosis. Lancet *377*, 942–955. https://doi.org/10.1016/S0140-6736(10)61156-7.
11. Van Damme, P., Robberecht, W., and Van Den Bosch, L. (2017). Modelling amyotrophic lateral sclerosis: progress and possibilities. Dis. Model. Mech. *10*, 537–549. https://doi.org/10.1242/dmm.029058.
12. Da Cruz, S., and Cleveland, D.W. (2011). Understanding the role of TDP-43 and FUS/TLS in ALS and beyond. Curr. Opin. Neurobiol. *21*, 904–919. https://doi.org/10.1016/j.conb.2011.05.029.
13. Fujimori, K., Ishikawa, M., Otomo, A., Atsuta, N., Nakamura, R., Akiyama, T., Hadano, S., Aoki, M., Saya, H., Sobue, G., and Okano, H. (2018). Modeling sporadic ALS in iPSC-derived motor neurons identifies a potential therapeutic agent. Nat. Med. *24*, 1579–1589. https://doi.org/10.1038/s41591-018-0140-5.
14. Han, T.W., Kato, M., Xie, S., Wu, L.C., Mirzaei, H., Pei, J., Chen, M., Xie, Y., Allen, J., Xiao, G., and McKnight, S.L. (2012). Cell-free formation of RNA granules: bound RNAs identify features and components of cellular assemblies. Cell *149*, 768–779. https://doi.org/10.1016/j.cell.2012.04.016.
15. Lagier-Tourenne, C., Polymenidou, M., and Cleveland, D.W. (2010). TDP-43 and FUS/TLS: emerging roles in RNA processing and neurodegeneration. Hum. Mol. Genet. *19*, R46–R64. https://doi.org/10.1093/hmg/ddq137.
16. Shang, Y., and Huang, E.J. (2016). Mechanisms of FUS mutations in familial amyotrophic lateral sclerosis. Brain Res. *1647*, 65–78. https://doi.org/10.1016/j.brainres.2016.03.036.
17. Tan, A.Y., and Manley, J.L. (2009). The TET family of proteins: functions and roles in disease. J. Mol. Cell Biol. *1*, 82–92. https://doi.org/10.1093/jmcb/mjp025.
18. Wang, X., Arai, S., Song, X., Reichart, D., Du, K., Pascual, G., Tempst, P., Rosenfeld, M.G., Glass, C.K., and Kurokawa, R. (2008). Induced ncRNAs allosterically modify RNA-binding proteins in cis to inhibit transcription. Nature *454*, 126–130. https://doi.org/10.1038/nature06992.
19. Lagier-Tourenne, C., Polymenidou, M., Hutt, K.R., Vu, A.Q., Baughn, M., Huelga, S.C., Clutario, K.M., Ling, S.-C., Liang, T.Y., Mazur, C., et al. (2012). Divergent roles of ALS-linked proteins FUS/TLS and TDP-43 intersect in processing long pre-mRNAs. Nat. Neurosci. *15*, 1488–1497. https://doi.org/10.1038/nn.3230.
20. Yu, Y., and Reed, R. (2015). FUS functions in coupling transcription to splicing by mediating an interaction between RNAP II and U1 snRNP. Proc. Natl. Acad. Sci. USA *112*, 8608–8613. https://doi.org/10.1073/pnas.1506282112.
21. Ishigaki, S., Masuda, A., Fujioka, Y., Iguchi, Y., Katsuno, M., Shibata, A., Urano, F., Sobue, G., and Ohno, K. (2012). Position-dependent FUS-RNA interactions regulate alternative splicing events and transcriptions. Sci. Rep. *2*, 529. https://doi.org/10.1038/srep00529.
22. Rogelj, B., Easton, L.E., Bogu, G.K., Stanton, L.W., Rot, G., Curk, T., Zupan, B., Sugimoto, Y., Modic, M., Haberman, N., et al. (2012). Widespread binding of FUS along nascent RNA regulates alternative splicing in the brain. Sci. Rep. *2*, 603. https://doi.org/10.1038/srep00603.
23. Masuda, A., Takeda, J.-I., Okuno, T., Okamoto, T., Ohkawara, B., Ito, M., Ishigaki, S., Sobue, G., and Ohno, K. (2015). Position-specific binding of FUS to nascent RNA regulates mRNA length. Genes Dev. *29*, 1045–1057. https://doi.org/10.1101/gad.255737.114.
24. Fujii, R., Okabe, S., Urushido, T., Inoue, K., Yoshimura, A., Tachibana, T., Nishikawa, T., Hicks, G.G., and Takumi, T. (2005). The RNA Binding Protein TLS Is Translocated to Dendritic Spines by mGluR5 Activation and Regulates Spine Morphology. Curr. Biol. *15*, 587–593. https://doi.org/10.1016/j.cub.2005.01.058.
25. Kanai, Y., Dohmae, N., and Hirokawa, N. (2004). Kinesin transports RNA: isolation and characterization of an RNA-transporting granule. Neuron *43*, 513–525. https://doi.org/10.1016/j.neuron.2004.07.022.
26. López-Erauskin, J., Tadokoro, T., Baughn, M.W., Myers, B., McAlonis-Downes, M., Chillon-Marinas, C., Asiaban, J.N., Artates, J., Bui, A.T., Vetto, A.P., et al. (2018). ALS/FTD-Linked Mutation in FUS Suppresses Intra- axonal Protein Synthesis and Drives Disease Without Nuclear Loss-of-Function of FUS. Neuron *100*, 816–830.e7. https://doi.org/10.1016/j.neuron.2018.09.044.
27. Sephton, C.F., Tang, A.A., Kulkarni, A., West, J., Brooks, M., Stubblefield, J.J., Liu, Y., Zhang, M.Q., Green, C.B., Huber, K.M., et al. (2014). Activity-dependent FUS dysregulation disrupts synaptic homeostasis. Proc. Natl. Acad. Sci. USA *111*, E4769–E4778. https://doi.org/10.1073/pnas.1406162111.
28. Yasuda, K., Zhang, H., Loiselle, D., Haystead, T., Macara, I.G., and Mili, S. (2013). The RNA-binding protein Fus directs translation of localized mRNAs in APC-RNP granules. J. Cell Biol. *203*, 737–746. https://doi.org/10.1083/jcb.201306058.dv.
29. Tan, A.Y., and Manley, J.L. (2010). TLS Inhibits RNA Polymerase III Transcription. Mol. Cell Biol. *30*, 186–196. https://doi.org/10.1128/MCB.00884-09.

30. Biscarini, S., Capauto, D., Peruzzi, G., Lu, L., Colantoni, A., Santini, T., Shneider, N.A., Caffarelli, E., Laneve, P., and Bozzoni, I. (2018). Characterization of the lncRNA transcriptome in mESC-derived motor neurons: Implications for FUS-ALS. Stem Cell Res. *27*, 172–179. https://doi.org/10.1016/j.scr.2018.01.037.
31. Morlando, M., Dini Modigliani, S., Torrelli, G., Rosa, A., Di Carlo, V., Caffarelli, E., and Bozzoni, I. (2012). FUS stimulates microRNA biogenesis by facilitating co-transcriptional Drosha recruitment. EMBO J. *31*, 4502–4510. https://doi.org/10.1038/emboj.2012.319.
32. Errichelli, L., Dini Modigliani, S., Laneve, P., Colantoni, A., Legnini, I., Capauto, D., Rosa, A., De Santis, R., Scarfò, R., Peruzzi, G., et al. (2017). FUS affects circular RNA expression in murine embryonic stem cell-derived motor neurons. Nat. Commun. *8*, 14741. https://doi.org/10.1038/ncomms14741.
33. Mastrocola, A.S., Kim, S.H., Trinh, A.T., Rodenkirch, L.A., and Tibbetts, R.S. (2013). The RNA-binding protein fused in sarcoma (FUS) functions downstream of poly(ADP-ribose) polymerase (PARP) in response to DNA damage. J. Biol. Chem. *288*, 24731–24741. https://doi.org/10.1074/jbc.M113.497974.
34. Wang, W.-Y., Pan, L., Su, S.C., Quinn, E.J., Sasaki, M., Jimenez, J.C., Mackenzie, I.R.A., Huang, E.J., and Tsai, L.-H. (2013). Interaction of FUS and HDAC1 regulates DNA damage response and repair in neurons. Nat. Neurosci. *16*, 1383–1391. https://doi.org/10.1038/nn.3514.
35. Hicks, G.G., Singh, N., Nashabi, A., Mai, S., Bozek, G., Klewes, L., Arapovic, D., White, E.K., Koury, M.J., Oltz, E.M., et al. (2000). Fus deficiency in mice results in defective B-lymphocyte development and activation, high levels of chromosomal instability and perinatal death. Nat. Genet. *24*, 175–179. https://doi.org/10.1038/72842.
36. Kuroda, M., Sok, J., Webb, L., Baechtold, H., Urano, F., Yin, Y., Chung, P., de Rooij, D.G., Akhmedov, A., Ashley, T., and Ron, D. (2000). Male sterility and enhanced radiation sensitivity in TLS(-/-) mice. EMBO J. *19*, 453–462. https://doi.org/10.1093/emboj/19.3.453.
37. Sugawara, T., Oguro, H., Negishi, M., Morita, Y., Ichikawa, H., Iseki, T., Yokosuka, O., Nakauchi, H., and Iwama, A. (2010). FET family proto-oncogene Fus contributes to self-renewal of hematopoietic stem cells. Exp. Hematol. *38*, 696–706. https://doi.org/10.1016/j.exphem.2010.04.006.
38. Ho, W.Y., Agrawal, I., Tyan, S.-H., Sanford, E., Chang, W.-T., Lim, K., Ong, J., Tan, B.S.Y., Moe, A.A.K., Yu, R., et al. (2021). Dysfunction in nonsense-mediated decay, protein homeostasis, mitochondrial function, and brain connectivity in ALS-FUS mice with cognitive deficits. Acta Neuropathol. Commun. *9*, 9. https://doi.org/10.1186/s40478-020-01111-4.
39. Tsai, Y.-L., Coady, T.H., Lu, L., Zheng, D., Alland, I., Tian, B., Shneider, N.A., and Manley, J.L. (2020). ALS/FTD-associated protein FUS induces mitochondrial dysfunction by preferentially sequestering respiratory chain complex mRNAs. Genes Dev. *34*, 785–805. https://doi.org/10.1101/gad.335836.119.
40. Sabatelli, M., Moncada, A., Conte, A., Lattante, S., Marangi, G., Luigetti, M., Lucchini, M., Mirabella, M., Romano, A., Del Grande, A., et al. (2013). Mutations in the 3′ untranslated region of FUS causing FUS overexpression are associated with amyotrophic lateral sclerosis. Hum. Mol. Genet. *22*, 4748–4755. https://doi.org/10.1093/hmg/ddt328.
41. Mitchell, J.C., McGoldrick, P., Vance, C., Hortobagyi, T., Sreedharan, J., Rogelj, B., Tudor, E.L., Smith, B.N., Klasen, C., Miller, C.C.J., et al. (2013). Overexpression of human wild-type FUS causes progressive motor neuron degeneration in an age- and dose-dependent fashion. Acta Neuropathol. *125*, 273–288. https://doi.org/10.1007/s00401-012-1043-z.
42. Ling, S.-C., Dastidar, S.G., Tokunaga, S., Ho, W.Y., Lim, K., Ilieva, H., Parone, P.A., Tyan, S.-H., Tse, T.M., Chang, J.-C., et al. (2019). Overriding FUS autoregulation in mice triggers gain-of-toxic dysfunctions in RNA metabolism and autophagy-lysosome axis. Elife *8*, e40811. https://doi.org/10.7554/eLife.40811.
43. Sleegers, K., Brouwers, N., Gijselinck, I., Theuns, J., Goossens, D., Wauters, J., Del-Favero, J., Cruts, M., van Duijn, C.M., and Van Broeckhoven, C. (2006). APP duplication is sufficient to cause early onset Alzheimer's dementia with cerebral amyloid angiopathy. Brain *129*, 2977–2983. https://doi.org/10.1093/brain/awl203.
44. Singleton, A.B., Farrer, M., Johnson, J., Singleton, A., Hague, S., Kachergus, J., Hulihan, M., Peuralinna, T., Dutra, A., Nussbaum, R., et al. (2003). α-Synuclein Locus Triplication Causes Parkinson's Disease. Science *302*, 841. https://doi.org/10.1126/science.1090278.
45. Ha, M., and Kim, V.N. (2014). Regulation of microRNA biogenesis. Nat. Rev. Mol. Cell Biol. *15*, 509–524. https://doi.org/10.1038/nrm3838.
46. Okamura, K., and Lai, E.C. (2008). Endogenous small interfering RNAs in animals. Nat. Rev. Mol. Cell Biol. *9*, 673–678. https://doi.org/10.1038/nrm2479.
47. Alles, J., Fehlmann, T., Fischer, U., Backes, C., Galata, V., Minet, M., Hart, M., Abu-Halima, M., Grässer, F.A., Lenhof, H.-P., et al. (2019). An estimate of the total number of true human miRNAs. Nucleic Acids Res. *47*, 3353–3364. https://doi.org/10.1093/nar/gkz097.
48. Kozomara, A., Birgaoanu, M., and Griffiths-Jones, S. (2019). miRBase: from microRNA sequences to function. Nucleic Acids Res. *47*, D155–D162. https://doi.org/10.1093/nar/gky1141.
49. Denli, A.M., Tops, B.B.J., Plasterk, R.H.A., Ketting, R.F., and Hannon, G.J. (2004). Processing of primary microRNAs by the Microprocessor complex. Nature *432*, 231–235. https://doi.org/10.1038/nature03049.
50. Gregory, R.I., Yan, K.P., Amuthan, G., Chendrimada, T., Doratotaj, B., Cooch, N., and Shiekhattar, R. (2004). The Microprocessor complex mediates the genesis of microRNAs. Nature *432*, 235–240. https://doi.org/10.1038/nature03120.
51. Siomi, H., and Siomi, M.C. (2010). Posttranscriptional Regulation of MicroRNA Biogenesis in Animals. Mol. Cell *38*, 323–332. https://doi.org/10.1016/j.molcel.2010.03.013.
52. Sun, S., Ling, S.-C., Qiu, J., Albuquerque, C.P., Zhou, Y., Tokunaga, S., Li, H., Qiu, H., Bui, A., Yeo, G.W., et al. (2015). ALS-causative mutations in FUS/TLS confer gain and loss of function by altered association with SMN and U1-snRNP. Nat. Commun. *6*, 6171. https://doi.org/10.1038/ncomms7171.
53. Zhang, T., Wu, Y.-C., Mullane, P., Ji, Y.J., Liu, H., He, L., Arora, A., Hwang, H.-Y., Alessi, A.F., Niaki, A.G., et al. (2018). FUS Regulates Activity of MicroRNA-Mediated Gene Silencing. Mol. Cell *69*, 787–801.e8. https://doi.org/10.1016/j.molcel.2018.02.001.
54. Dini Modigliani, S., Morlando, M., Errichelli, L., Sabatelli, M., and Bozzoni, I. (2014). An ALS-associated mutation in the FUS 3′-UTR disrupts a microRNA-FUS regulatory circuitry. Nat. Commun. *5*, 4335. https://doi.org/10.1038/ncomms5335.
55. Zhou, Y., Liu, S., Liu, G., Oztürk, A., and Hicks, G.G. (2013). ALS-associated FUS mutations result in compromised FUS alternative splicing and autoregulation. PLoS Genet. *9*, e1003895. https://doi.org/10.1371/journal.pgen.1003895.
56. Kozomara, A., and Griffiths-Jones, S. (2014). miRBase: annotating high confidence microRNAs using deep sequencing data. Nucl. Acids Res. *42*, D68–D73. https://doi.org/10.1093/nar/gkt1181.
57. Pearson, J.C., Lemons, D., and McGinnis, W. (2005). Modulating Hox gene functions during animal body patterning. Nat. Rev. Genet. *6*, 893–904. https://doi.org/10.1038/nrg1726.
58. Yekta, S., Tabin, C.J., and Bartel, D.P. (2008). MicroRNAs in the Hox network: an apparent link to posterior prevalence. Nat. Rev. Genet. *9*, 789–796. https://doi.org/10.1038/nrg2400.
59. Yekta, S., Shih, I.H., and Bartel, D.P. (2004). MicroRNA-Directed Cleavage of HOXB8 mRNA. Science *304*, 594–596. https://doi.org/10.1126/science.1097434.
60. Friedländer, M.R., Mackowiak, S.D., Li, N., Chen, W., and Rajewsky, N. (2012). miRDeep2 accurately identifies known and hundreds of novel microRNA genes in seven animal clades. Nucleic Acids Res. *40*, 37–52. https://doi.org/10.1093/nar/gkr688.
61. Berezikov, E., Robine, N., Samsonova, A., Westholm, J.O., Naqvi, A., Hung, J.-H., Okamura, K., Dai, Q., Bortolamiol-Becet, D., Martin, R., et al. (2011). Deep annotation of Drosophila melanogaster microRNAs yields insights into their processing, modification, and emergence. Genome Res. *21*, 203–215. https://doi.org/10.1101/gr.116657.110.
62. Ladewig, E., Okamura, K., Flynt, A.S., Westholm, J.O., and Lai, E.C. (2012). Discovery of hundreds of mirtrons in mouse and human small RNA data. Genome Res. *22*, 1634–1645. https://doi.org/10.1101/gr.133553.111.
63. Auyeung, V.C., Ulitsky, I., McGeary, S.E., and Bartel, D.P. (2013). Beyond Secondary Structure: Primary-Sequence Determinants License Pri-miRNA Hairpins for Processing. Cell *152*, 844–858. https://doi.org/10.1016/j.cell.2013.01.031.
64. Kwon, S.C., Baek, S.C., Choi, Y.-G., Yang, J., Lee, Y.S., Woo, J.-S., and Kim, V.N. (2019). Molecular Basis for the Single-Nucleotide Precision of Primary microRNA Processing. Mol. Cell *73*, 505–518.e5. https://doi.org/10.1016/j.molcel.2018.11.005.
65. Seitz, H., Royo, H., Bortolin, M.L., Lin, S.P., Ferguson-Smith, A.C., and Cavaillé, J. (2004). A Large Imprinted microRNA Gene Cluster at the Mouse Dlk1-Gtl2 Domain.

Genome Res. *14*, 1741–1748. https://doi.org/10.1101/gr.2743304.
66. Winter, J. (2015). MicroRNAs of the miR379–410 cluster: New players in embryonic neurogenesis and regulators of neuronal function. Neurogenesis *2*, e1004970–e1004979. https://doi.org/10.1080/23262133.2015.1004970.
67. Agarwal, V., Bell, G.W., Nam, J.-W., and Bartel, D.P. (2015). Predicting effective microRNA target sites in mammalian mRNAs. Elife *4*, e05005. https://doi.org/10.7554/eLife.05005.
68. Eyers, P.A., Keeshan, K., and Kannan, N. (2017). Tribbles in the 21st Century: The Evolving Roles of Tribbles Pseudokinases in Biology and Disease. Trends Cell Biol. *27*, 284–298. https://doi.org/10.1016/j.tcb.2016.11.002.
69. Tan, S.H., Yam, A.W.Y., Lawton, L.N., Wong, R.W.J., Young, R.A., Look, A.T., and Sanda, T. (2016). TRIB2 reinforces the oncogenic transcriptional program controlled by the TAL1 complex in T-cell acute lymphoblastic leukemia. Leukemia *30*, 959–962. https://doi.org/10.1038/leu.2015.195.
70. Foulkes, D.M., Byrne, D.P., Yeung, W., Shrestha, S., Bailey, F.P., Ferries, S., Eyers, C.E., Keeshan, K., Wells, C., Drewry, D.H., et al. (2018). Covalent inhibitors of EGFR family protein kinases induce degradation of human Tribbles 2 (TRIB2) pseudokinase in cancer cells. Sci. Signal. *11*, eaat7951. https://doi.org/10.1126/scisignal.aat7951.
71. Hill, R., Madureira, P.A., Ferreira, B., Baptista, I., Machado, S., Colaço, L., dos Santos, M., Liu, N., Dopazo, A., Ugurel, S., et al. (2017). TRIB2 confers resistance to anti-cancer therapy by activating the serine/threonine protein kinase AKT. Nat. Commun. *8*, 14687. https://doi.org/10.1038/ncomms14687.
72. Kim, Y.-E., Oh, K.-W., Kwon, M.-J., Choi, W.-J., Oh, S.i., Ki, C.-S., and Kim, S.H. (2015). De novo FUS mutations in 2 Korean patients with sporadic amyotrophic lateral sclerosis. Neurobiol. Aging *36*, 1604.e17–1604.e19. https://doi.org/10.1016/j.neurobiolaging.2014.10.002.
73. Lim, S.M., Choi, W.-J., Oh, K.-W., Xue, Y., Choi, J.Y., Kim, S.H., Nahm, M., Kim, Y.-E., Lee, J., Noh, M.-Y., et al. (2016). Directly converted patient-specific induced neurons mirror the neuropathology of FUS with disrupted nuclear localization in amyotrophic lateral sclerosis. Mol. Neurodegener. *11*, 8. https://doi.org/10.1186/s13024-016-0075-6.
74. Hor, J.-H., Santosa, M.M., Lim, V.J.W., Ho, B.X., Taylor, A., Khong, Z.J., Ravits, J., Fan, Y., Liou, Y.-C., Soh, B.-S., and Ng, S.Y. (2021). ALS motor neurons exhibit hallmark metabolic defects that are rescued by SIRT3 activation. Cell Death Differ. *28*, 1379–1397. https://doi.org/10.1038/s41418-020-00664-0.
75. Treiber, T., Treiber, N., and Meister, G. (2019). Regulation of microRNA biogenesis and its crosstalk with other cellular pathways. Nat. Rev. Mol. Cell Biol. *20*, 5–20. https://doi.org/10.1038/s41580-018-0059-1.
76. Nussbacher, J.K., and Yeo, G.W. (2018). Systematic Discovery of RNA Binding Proteins that Regulate MicroRNA Levels. Mol. Cell *69*, 1005–1016.e7. https://doi.org/10.1016/j.molcel.2018.02.012.
77. Treiber, T., Treiber, N., Plessmann, U., Harlander, S., Daiß, J.L., Eichner, N., Lehmann, G., Schall, K., Urlaub, H., and Meister, G. (2017). A Compendium of RNA-Binding Proteins that Regulate MicroRNA Biogenesis. Mol. Cell *66*, 270–284.e13. https://doi.org/10.1016/j.molcel.2017.03.014.
78. Fiore, R., Khudayberdiev, S., Christensen, M., Siegel, G., Flavell, S.W., Kim, T.-K., Greenberg, M.E., and Schratt, G. (2009). Mef2-mediated transcription of the miR379–410 cluster regulates activity-dependent dendritogenesis by fine-tuning Pumilio2 protein levels. EMBO J. *28*, 697–710. https://doi.org/10.1038/emboj.2009.10.
79. Rago, L., Beattie, R., Taylor, V., and Winter, J. (2014). miR379-410 cluster miRNAs regulate neurogenesis and neuronal migration by fine-tuning N-cadherin. EMBO J. *33*, 906–920. https://doi.org/10.1002/embj.201386591.
80. Marty, V., Labialle, S., Bortolin-Cavaillé, M.L., Ferreira De Medeiros, G., Moisan, M.-P., Florian, C., and Cavaillé, J. (2016). Deletion of the miR-379/miR-410 gene cluster at the imprinted *Dlk1-Dio3* locus enhances anxiety-related behaviour. Hum. Mol. Genet. *25*, 728–739. https://doi.org/10.1093/hmg/ddv510.
81. Yen, Y.-P., Hsieh, W.-F., Tsai, Y.-Y., Lu, Y.-L., Liau, E.S., Hsu, H.-C., Chen, Y.-C., Liu, T.-C., Chang, M., Li, J., et al. (2018). Dlk1-Dio3 locus-derived lncRNAs perpetuate postmitotic motor neuron cell fate and subtype identity. Elife *7*, e38080. https://doi.org/10.7554/eLife.38080.
82. Haramati, S., Chapnik, E., Sztainberg, Y., Eilam, R., Zwang, R., Gershoni, N., McGlinn, E., Heiser, P.W., Wills, A.-M., Wirguin, I., et al. (2010). miRNA malfunction causes spinal motor neuron disease. Proc. Natl. Acad. Sci. USA *107*, 13111–13116. https://doi.org/10.1073/pnas.1006151107.
83. Emde, A., Eitan, C., Liou, L.L., Libby, R.T., Rivkin, N., Magen, I., Reichenstein, I., Oppenheim, H., Eilam, R., Silvestroni, A., et al. (2015). Dysregulated mi RNA biogenesis downstream of cellular stress and ALS -causing mutations: a new mechanism for ALS. EMBO J. *34*, 2633–2651. https://doi.org/10.15252/embj.201490493.
84. Amin, N.D., Bai, G., Klug, J.R., Bonanomi, D., Pankratz, M.T., Gifford, W.D., Hinckley, C.A., Sternfeld, M.J., Driscoll, S.P., Dominguez, B., et al. (2015). Loss of motoneuron-specific microRNA-218 causes systemic neuromuscular failure. Science *350*, 1525–1529. https://doi.org/10.1126/science.aad2509.
85. Hoye, M.L., Koval, E.D., Wegener, A.J., Hyman, T.S., Yang, C., O'Brien, D.R., Miller, R.L., Cole, T., Schoch, K.M., Shen, T., et al. (2017). MicroRNA Profiling Reveals Marker of Motor Neuron Disease in ALS Models. J. Neurosci. *37*, 5574–5586. https://doi.org/10.1523/JNEUROSCI.3582-16.2017.
86. Bhinge, A., Namboori, S.C., Bithell, A., Soldati, C., Buckley, N.J., and Stanton, L.W. (2016). MiR-375 is Essential for Human Spinal Motor Neuron Development and May Be Involved in Motor Neuron Degeneration: MiR-375, A REST Target, Specifies Motor Neurons. Stem Cell. *34*, 124–134. https://doi.org/10.1002/stem.2233.
87. Reichenstein, I., Eitan, C., Diaz-Garcia, S., Haim, G., Magen, I., Siany, A., Hoye, M.L., Rivkin, N., Olender, T., Toth, B., et al. (2019). Human genetics and neuropathology suggest a link between miR-218 and amyotrophic lateral sclerosis pathophysiology. Sci. Transl. Med. *11*, eaav5264. https://doi.org/10.1126/scitranslmed.aav5264.
88. Tung, Y.-T., Peng, K.-C., Chen, Y.-C., Yen, Y.-P., Chang, M., Thams, S., and Chen, J.-A. (2019). Mir-17∼92 Confers Motor Neuron Subtype Differential Resistance to ALS-Associated Degeneration. Cell Stem Cell *25*, 193–209.e7. https://doi.org/10.1016/j.stem.2019.04.016.
89. Nishimura, A.L., Mitne-Neto, M., Silva, H.C.A., Richieri-Costa, A., Middleton, S., Cascio, D., Kok, F., Oliveira, J.R.M., Gillingwater, T., Webb, J., et al. (2004). A Mutation in the Vesicle-Trafficking Protein VAPB Causes Late-Onset Spinal Muscular Atrophy and Amyotrophic Lateral Sclerosis. Am. J. Hum. Genet. *75*, 822–831. https://doi.org/10.1086/425287.
90. Casci, I., Krishnamurthy, K., Kour, S., Tripathy, V., Ramesh, N., Anderson, E.N., Marrone, L., Grant, R.A., Oliver, S., Gochenaur, L., et al. (2019). Muscleblind acts as a modifier of FUS toxicity by modulating stress granule dynamics and SMN localization. Nat. Commun. *10*, 5583. https://doi.org/10.1038/s41467-019-13383-z.
91. Capauto, D., Colantoni, A., Lu, L., Santini, T., Peruzzi, G., Biscarini, S., Morlando, M., Shneider, N.A., Caffarelli, E., Laneve, P., and Bozzoni, I. (2018). A Regulatory Circuitry Between Gria2, miR-409, and miR-495 Is Affected by ALS FUS Mutation in ESC-Derived Motor Neurons. Mol. Neurobiol. *55*, 7635–7651. https://doi.org/10.1007/s12035-018-0884-4.
92. De Santis, R., Santini, L., Colantoni, A., Peruzzi, G., de Turris, V., Alfano, V., Bozzoni, I., and Rosa, A. (2017). FUS Mutant Human Motoneurons Display Altered Transcriptome and microRNA Pathways with Implications for ALS Pathogenesis. Stem Cell Rep. *9*, 1450–1462. https://doi.org/10.1016/j.stemcr.2017.09.004.
93. Figueroa-Romero, C., Hur, J., Lunn, J.S., Paez-Colasante, X., Bender, D.E., Yung, R., Sakowski, S.A., and Feldman, E.L. (2016). Expression of microRNAs in human post-mortem amyotrophic lateral sclerosis spinal cords provides insight into disease mechanisms. Mol. Cell. Neurosci. *71*, 34–45. https://doi.org/10.1016/j.mcn.2015.12.008.
94. Li, M., Ona, V.O., Guégan, C., Chen, M., Jackson-Lewis, V., Andrews, L.J., Olszewski, A.J., Stieg, P.E., Lee, J.P., Przedborski, S., and Friedlander, R.M. (2000). Functional Role of Caspase-1 and Caspase-3 in an ALS Transgenic Mouse Model. Science *288*, 335–339. https://doi.org/10.1126/science.288.5464.335.
95. Sathasivam, S., and Shaw, P.J. (2005). Apoptosis in amyotrophic lateral sclerosis—what is the evidence? Lancet Neurol. *4*, 500–509. https://doi.org/10.1016/S1474-4422(05)70142-3.
96. Reyes, N.A., Fisher, J.K., Austgen, K., VandenBerg, S., Huang, E.J., and Oakes, S.A. (2010). Blocking the mitochondrial apoptotic pathway preserves motor neuron viability and function in a mouse model of amyotrophic lateral sclerosis. J. Clin. Invest. *120*, 3673–3679. https://doi.org/10.1172/JCI42986.
97. Zhu, S., Stavrovskaya, I.G., Drozda, M., Kim, B.Y.S., Ona, V., Li, M., Sarang, S., Liu, A.S., Hartley, D.M., Wu, D.C., et al. (2002).

Minocycline inhibits cytochrome c release and delays progression of amyotrophic lateral sclerosis in mice. Nature *417*, 74–78. https://doi.org/10.1038/417074a.

98. Wu, C., Watts, M.E., and Rubin, L.L. (2019). MAP4K4 Activation Mediates Motor Neuron Degeneration in Amyotrophic Lateral Sclerosis. Cell Rep. *26*, 1143–1156.e5. https://doi.org/10.1016/j.celrep.2019.01.019.
99. Soffietti, R., Ahluwalia, M., Lin, N., and Rudà, R. (2020). Management of brain metastases according to molecular subtypes. Nat. Rev. Neurol. *16*, 557–574. https://doi.org/10.1038/s41582-020-0391-x.
100. Swarup, V., Hinz, F.I., Rexach, J.E., Noguchi, K.I., Toyoshiba, H., Oda, A., Hirai, K., Sarkar, A., Seyfried, N.T., Cheng, C., et al. (2019). Identification of evolutionarily conserved gene networks mediating neurodegenerative dementia. Nat. Med. *25*, 152–164. https://doi.org/10.1038/s41591-018-0223-3.
101. Langmead, B., Trapnell, C., Pop, M., and Salzberg, S.L. (2009). Ultrafast and memory-efficient alignment of short DNA sequences to the human genome. Genome Biol. *10*, R25. https://doi.org/10.1186/gb-2009-10-3-r25.
102. Friedländer, M.R., Mackowiak, S.D., Li, N., Chen, W., and Rajewsky, N. (2012). miRDeep2 accurately identifies known and hundreds of novel microRNA genes in seven animal clades. Nucleic Acids Res. *40*, 37–52. https://doi.org/10.1093/nar/gkr688.
103. Robinson, M.D., and Oshlack, A. (2010). A scaling normalization method for differential expression analysis of RNA-seq data. Genome Biol. *11*, R25. https://doi.org/10.1186/gb-2010-11-3-r25.
104. Robinson, M.D., McCarthy, D.J., and Smyth, G.K. (2010). edgeR: a Bioconductor package for differential expression analysis of digital gene expression data. Bioinformatics *26*, 139–140. https://doi.org/10.1093/bioinformatics/btp616.
105. Zuker, M. (2003). Mfold web server for nucleic acid folding and hybridization prediction. Nucleic Acids Res. *31*, 3406–3415. https://doi.org/10.1093/nar/gkg595.
106. Ling, S.-C., Albuquerque, C.P., Han, J.S., Lagier-Tourenne, C., Tokunaga, S., Zhou, H., and Cleveland, D.W. (2010). ALS-associated mutations in TDP-43 increase its stability and promote TDP-43 complexes with FUS/TLS. Proc. Natl. Acad. Sci. USA *107*, 13318–13323. https://doi.org/10.1073/pnas.1008227107.

STAR★METHODS

KEY RESOURCES TABLE

REAGENT or RESOURCE	SOURCE	IDENTIFIER
Antibodies		
Mouse monoclonal anti-FUS (clone 4H11)	Santa Cruz Biotech	cat#: sc-47711, RRID: AB_2105208
Goat polyclonal anti-HA	Bethyl Laboratories, Inc.,	cat#: A190-238A; RRID: AB_2631898
Mouse monoclonal anti-GAPDH (clone 1E6D9)	Proteintech	cat#: 60004-1-Ig; RRID: AB_2107436
Mouse monoclonal anti-GAPDH (clone 6C5)	Abcam	cat#: ab8245; RRID: AB_2107448
Rabbit polyclonal anti-TRIB2	Proteintech	cat#: 15359-1-AP; RRID: AB_2209083
Rabbit monoclonal anti-ISLET1	Abcam	cat#: ab109517; RRID: AB_10866454
Rabbit polyclonal anti-P62/sequestosome	Bethyl Laboratories, Inc.,	cat#: A302-855A; RRID: AB_10631130
Rabbit monoclonal AKT (clone C67E7)	Cell Signaling Technology	cat#: 4691; RRID: AB_915783
Rabbit monoclonal Phospho-AKT (T308) (clone D25E6)	Cell Signaling Technology	cat#: 13038; RRID: AB_2629447
Biological samples		
BJ-iPS iPSC	Ng et al. (2015)	N/A
18a iPSC	Eggan Lab, Boulting et al. (2011)	N/A
29days iPSC ($SOD1^{L144F}$)	Eggan Lab, Boulting et al. (2011)	N/A
47a iPSC ($TDP43^{G298S}$)	Eggan Lab, Rodriguez-Muela et al. (2017)	N/A
19f iPSC (C9ORF72)	Eggan Lab, Kiskinis et al. (2014)	N/A
CS14isALS-Tn16 (sALS1) iPSC	Cedars-Sinai Medical Center's	CS14isALS-Tn16
CS89isALS-Tn16 (sALS3) iPSC	Cedars-Sinai Medical Center's	CS89isALS-Tn16
Postmortem human tissues	Hanyang University Hospital	IRB# 2011-R-63
Postmortem human tissues	University of California, San Diego (UCSD)	UCSDIRB #20056
Postmortem human tissues	Benaroya Research Institute, Seattle, WA	IRB #10058
Chemicals, peptides, and recombinant proteins		
TAK-285	MedChem Express	HY-15196-10 mM
lapatinib	MedChem Express	HY-50898-50 mg
Critical commercial assays		
TruSeq Small RNA Library Prep Kit	Illumina	RS-200
Dual-Glo Luciferase assay system	Promega	E2940
Deposited data		
Raw FASTQ files for miRNA-sequencing libraries	SRA	SRP133090
Raw FASTQ files for miRNA-sequencing libraries	NCBI's BioProject	ID:PRJNA434631
Experimental models: Cell lines		
Neuro2A (*Mus musculus*)	ATCC	CCL-131
TRex Flp-In HeLa (*Homo sapines*)	Ling et al., PNAS 2010	N/A
Experimental models: Organisms/strains		
Mouse/B6N.Cg-Tg(Prnp-FUS-wt) line 101	Ling et al., eLife 2019	N/A

(*Continued on next page*)

Continued

REAGENT or RESOURCE	SOURCE	IDENTIFIER
Oligonucleotides		
Mouse Trib2 RT-qPCR primer (forward) 5′- CTCTCCTACTTCTGGGTGGC-3′	IDT oligos	N/A
Mouse Trib2 RT-qPCR primer (reverse) 5′- CACTCTTGTCTCCCGATGCC-3′	IDT oligos	N/A
Mouse Vapb RT-qPCR primer (forward) 5′- TGCATCCAAGACAGAAGCAC -3′	IDT oligos	N/A
Mouse Vapb RT-qPCR primer (reverse) 5′- GCCTTCCTCACCCGAAGT -3′	IDT oligos	N/A
Mouse Mbnl1 RT-qPCR primer (forward) 5′- CACTGTGTCCGCAGCAAC -3′	IDT oligos	N/A
Mouse Mbnl1 RT-qPCR primer (reverse) 5′- GCCTTCCTCACCCGAAGT -3′	IDT oligos	N/A
Mouse Ubap2 RT-qPCR primer (forward) 5′- CGTTCCTGCACATCATGC -3′	IDT oligos	N/A
Mouse Ubap2 RT-qPCR primer (reverse) 5′- CTTGAGACTTGGGCTGAAGG -3′	IDT oligos	N/A
Mouse Cyp26b1 RT-qPCR primer (forward) 5′- AGACTCTTCACGCCCGTCT -3′	IDT oligos	N/A
Mouse Cyp26b1 RT-qPCR primer (reverse) 5′- CGTGAGTGTCTCGGATGCTA -3′	IDT oligos	N/A
Mouse Slc25a42 RT-qPCR primer (forward) 5′- TATGCGGGACTCAGCTTCTT -3′	IDT oligos	N/A
Mouse Slc25a42 RT-qPCR primer (reverse) 5′- GTGACACCTGCTGTCTGCAT -3′	IDT oligos	N/A
Mouse GAPDH RT-qPCR primer (forward) 5′- CATGGCCTTCCGTGTTCCTA -3′	IDT oligos	N/A
Mouse GAPDH RT-qPCR primer (reverse) 5′- CCTGCTTCACCACCTTCTTGAT -3′	IDT oligos	N/A
Mouse actin RT-qPCR primer (forward) 5′- CGTGGGCCGCCCTAGGCACCAG -3′	IDT oligos	N/A
Mouse actin RT-qPCR primer (reverse) 5′- TTGGCCTTAGGGTTCAGGGGGG -3′	IDT oligos	N/A
Recombinant DNA		
psiCHECK	Promega	
psCHECK-miR-1197-3p sensor	this study	N/A
psCHECK-miR-323-3p sensor	this study	N/A
psCHECK-miR-323-3p sensor	this study	N/A
psCHECK-miR-410-3p sensor	this study	N/A
psCHECK-miR-496-3p sensor	this study	N/A
psCHECK-Trib2-3′UTR-wild type	this study	N/A
psCHECK-Trib2-3′UTR-mut1	this study	N/A
psCHECK-Trib2-3′UTR-mut2	this study	N/A
psCHECK-Trib2-3′UTR-mut1+2	this study	N/A
psCHECK-Mbnl-3′UTR-wild type	this study	N/A
psCHECK-Mbnl-3′UTR-mut1	this study	N/A
psCHECK-Mbnl-3′UTR-mut2	this study	N/A
psCHECK-Mbnl-3′UTR-mut1+2	this study	N/A

(*Continued on next page*)

Continued

REAGENT or RESOURCE	SOURCE	IDENTIFIER
psCHECK-Vapb-3′UTR-wild type	this study	N/A
psCHECK-Vapb-3′UTR-mut	this study	N/A
psCHECK-Cyp26b1-3′UTR-wild type	this study	N/A
psCHECK-Cyp26b1-3′UTR-mut	this study	N/A
psCHECK-Klf11-3′UTR-wild type	this study	N/A
psCHECK-Klf11-3′UTR-mut	this study	N/A
psCHECK-Ubap2-3′UTR-wild type	this study	N/A
psCHECK-Ubap2-3′UTR-mut	this study	N/A
psCHECK-Slc25a42-3′UTR-wild type	this study	N/A
psCHECK-Slc25a42-3′UTR-mut1	this study	N/A
psCHECK-Slc25a42-3′UTR-mut2	this study	N/A
psCHECK-Slc25a42-3′UTR-mut1+2	this study	N/A
Software and algorithms		
FASTX-Toolkit	http://hannonlab.cshl.edu/fastx toolkit/index.html	
bowtie	Langmead et al. 2009,[101] https://doi.org/10.1186/gb-2009-10-3-r25	
Mirdeep2	Friedländer et al. 2011,[102] https://doi.org/10.1093/nar/gkr688	
edgeR	Robinson et al. 2010,[103,104] https://doi.org/10.1093/bioinformatics/btp616	
TargetScan	Agarwal et al. 2015,[67] https://doi.org/10.7554/eLife.05005	
mfold	Zuker 2003,[105] https://doi.org/10.1093/nar/gkg595	

RESOURCE AVAILABILITY

Lead contact

Further information and requests for resources and reagents should be directed to and will be fulfilled by the lead contact, Shuo-Chien Ling (phsling@nus.edu.sg or shuochien@gmail.com).

Material availability

Plasmids generated in this study will be deposited to Addgene.

Data and code availability

- Data
  Raw FASTQ files for miRNA-sequencing libraries were deposited at into SRA, with accession number SRP133090. This data has been deposited in NCBI's BioProject with ID:PRJNA434631 and are publicly available as of the date of publication. Accession numbers are listed in the key resources table. Raw data have been deposited at Mendeley and are publicly available as of the date of publication. DOIs are listed in the key resources table. Microscopy data reported in this paper will be shared by the lead contact upon request.
- Code
  This paper does not report original code.
- All other items
  Any additional information required to reanalyze the data reported in this paper is available from the lead contact upon request.

EXPERIMENTAL MODEL AND STUDY PARTICIPANT DETAILS

Mouse models

All studies were carried out under protocols approved by the National University of Singapore's Institutional Animal Care and Use Committee (IACUC), and were in compliance with Association for Assessment of Laboratory Animal Care (AAALAC) guidelines for animal use. All mice

used in this study were maintained at C57BL/6J background and were housed in groups in individually ventilated cages under a 12:12-h light/dark cycle with access to food and water *ad libitum*. Because there is no apparent gender bias to the overserved phenotypes and pathology, female and male mice are included and randomly allocated to experimental groups according to age and genotype. 4-weeks old mice were used in this study. No animals or samples were excluded in any of the experiments. FUS transgenic mice were generated using murine prion promoter to drive human FUS cDNA as described previously.[42] Mice were backcrossed to C57BL/6 for more than 10 generations and used for analysis in this paper. For genotyping, genomic DNA was isolated from tail biopsies using salt extraction methods and subjected to routine PCR methods using the following primers:

FUS transgene: 5′-GAGGATTTCCCAGTGGAGGT-3′ and 5′-CTCCATCAAAGGGACCTGAA-3′

FUS transgene insertion site: 5′-GGTGTTCCTGGAGGAGATGA-3′, 5′-CATGTTGACCTGGGACACTG-3′, and 5′-AGAGGGCATTCCC TTTGTCT-3′

Ethics approval and consent to participate

Human tissues used in this study came from Professor John Ravits and Professor Seung Hyun Kim, and the protocols were approved from their respective institution detailed below. Human tissue acquisition protocols followed HIPAA-compliant informed consent procedures and were approved by Institutional Review Boards and came from two sources, the University of California, San Diego (UCSD) (UCSDIRB #20056) and Benaroya Research Institute, Seattle, WA (IRB #10058), and distributed by material transfer agreement (Professor John Ravits). The Institutional Review Board of Hanyang University Hospital approved the study protocol, and written informed consent was obtained from all patients involved in the study (IRB# 2011-R-63) (Professor Seung Hyun Kim).

METHOD DETAILS

RNA extraction and quantitative RT-PCR

Total RNAs were extracted from the spinal cord tissues using Trizol reagent (Invitrogen) according to the manufacturer's instruction. After DNase treatment using RQ1 RNase-Free DNase (Promega), 1 μg RNA was reversely transcribed using Maxima First Strand cDNA Synthesis Kit for RT-qPCR (Thermo Fisher Scientific). mRNA levels were determined using Maxima SYBR Green qPCR master mix (Thermo Fisher Scientific). qRT-PCR primers for genes of interest were listed in key resouces table.

miRNAs quantification was performed with stem-loop real-time PCR according to the manufacturer's protocols using miRNA specific stem-loop primer probes (Applied Biosystems, and MiRXES). Both reverse transcription and qPCRs were performed in triplicate in three separate experiments on a QuantStudio 6 Flex Real-Time PCR System. U6 was used as an internal calibrator.

miRNA-seq library preparation and sequencing, and bioinformatics analysis

miRNA-seq libraries were prepared using TruSeq Small RNA kit (Illumina) according to the instructions. One μg total RNA was used for library construction, and after 15 cycles of PCR amplification, the resulting PCR products with small RNA inserts were size selected on a 6% native acrylamide gel. DNA was eluted from gel pieces in water and the quality and quantity of the libraries were checked by Bioanalyzer (Agilent Genomics). The libraries were sequenced on either Hiseq2000 (for spinal cord libraries) or Hiseq4000 (for hippocampus libraries) at Beijing Genomics Institute (BGI, Hong Kong). Raw FASTQ files for miRNA-sequencing libraries were deposited at into SRA, with accession number SRP133090.

Sequencing data were quality checked by FastQC and adaptors trimmed by Fastx_clipper from the FASTX-Toolkit package (http://hannonlab.cshl.edu/fastxtoolkit/index.html) to remove the Illumina 3′-adaptor sequence (TGGAATTCTCGGGTGCCAAGG). Reads with length 18-30 nt were mapped to the mm10 mouse genome assembly using bowtie v1[101] and perfectly mapping reads were counted. To count the corresponding miRNA reads, they were mapped onto mature miRNA sequences annotated in miRBase v21.[56] Read counts were first normalized by number of positions the read could be mapped to in the mouse genome sequence. Mirdeep2 pipeline was used for identification of novel miRNAs.[60] To require stricter evidence for processing by specific processing machineries, we set the following criteria for novel miRNA genes: a) more than 50 reads mapping to the hairpin, b) more than 5 star reads (total from the −5 to +5 range), c) Reads with top 2 most abundant 5′ ends in each arm constitute >95% of reads mapping to each arm of the hairpin. Candidate hairpins were then folded with mfold[105] and manually checked for microprocessor recognition motifs.[63] To analyze miRNA expression changes between samples, further read normalization for library size by TMM[103] and statistical analyses were done using edgeR.[104] miRNAs were filtered on expression criteria of minimum 1 cpm in at least 1 library and differentially expressed miRNAs were selected at $p < 0.05$, FDR (BH) adjusted p value. The PCA plot was drawn using the sklearn Python package. A pseudocount of 1 was added to the cpm normalized values. To avoid fluctuations of low read count genes, genes with the mean RPM of all libraries <3 were removed. 439 genes satisfied this criteria and log-transformed values were scaled and used for PCA.

Immunohistochemistry

Mice were anesthetized with isofluorane and perfused transcardially with phosphate buffered saline (PBS), followed by 4% paraformaldehyde (PFA) in phosphate buffer for fixation. The spinal cord and brain were dissected and post-fixed in 4% PFA in PBS for 2 h. Tissues were cryopreserved in 30% sucrose for over 24 h and embedded in Tissue-Tek before sectioning. Lumbar spinal cords and brain were sectioned at 30 and 35 μm, respectively, using a cryostat or microtome.[42]

For spinal cord and hippocampal sections staining, after three washes with 1xPBS, tissue sections were permeabilized in 0.3% Triton X-100 in 1xPBS for 5 min. The permeabilization steps were repeated twice. Primary blocking buffer containing 5% BSA and 0.5% Tween 20 in 1xPBS was used for blocking and incubation with primary antibodies. After blocking at room temperature for 1 h, the sections were incubated with primary antibodies at 4° overnight. The antibodies used in this study were FUS (Santa Cruz Biotechnology, clone 4H11, sc-47711) and p62 (Bethyl Laboratories, A302-855A), and listed in Table S5. Sections were carefully washed with 1xPBS for 3 times, 5 min each. Tissue sections were incubated with secondary antibodies conjugated with Alexa Fluor 488-, 568, 643 (1:1000, Thermo Fisher Scientific) and 1 μg/mL DAPI diluted in secondary blocking buffer containing 2% BSA and 0.5% Tween 20 in 1xPBS, and at room temperature for 1 h in the dark. The sections were then washed and mounted onto slides with Prolong Gold anti-fade reagent (Thermo Fisher Scientific, P36930).

Image acquisition

Confocal images were acquired using Zeiss LSM700 inverted confocal microscope with 4 laser lines (405/488/555/639 nm) at either a 20x/0.8 N.A. air or 63x/1.15 N.A. oil immersion objectives. Images were captured using an AxioCam MRm monochromatic CCD camera (Zeiss) run by Zeiss Zen software.

Immunoblotting

Spinal cords and hippocampi were harvested and snap froze in liquid nitrogen before protein extraction. RIPA buffer containing 15 mM NaCl, 1% Triton X-100, 0.5% sodium deoxycholate, 0.1% SDS, 50 mM Tris at pH8.0 was prepared and protease inhibitor (Thermo Fisher Scientific, 88266) was added before use. Tissues were homogenized in RIPA buffer and incubated at 4° for 2 h with gentle agitation. After incubation, lysed samples were centrifuged at 4°C for 30 min at 20,000 *xg* using a desktop centrifuge and the supernatant were collected for BCA protein concentration measurement (Thermo Fisher Scientific, 23225). Thirty μg of total protein for each sample was loaded for 10% SDS-PAGE. Proteins were transferred to PVDF membrane using 1x transfer buffer containing 1x Tris-Glycine (0.025 M Tris base and 0.192 M glycine) and 20% methanol at 100V for 90 min. Membranes were blocked using 5% milk in 1x TBST (50 mM Tris, 150 mM NaCl, 0.1% Tween 20, pH 7.4) at room temperature for 1 h. After blocking, membranes were incubated with primary antibodies at 4°C overnight. The primary antibodies used in this study were FUS (Santa Cruz Biotechnology, clone 4H11, sc-47711), HA (Bethyl Laboratories, A190-238A), GAPDH (Proteintech, 60004-1-Ig), Trib2 (Proteintech, 15359-1-AP) and listed in Table S3. Membranes were washed with 1XTBST and incubated with appropriate HRP-conjugated secondary antibodies (1:1000, Thermo Fisher Scientific) at room temperature for 1 h. After washing with 1xTBST extensively, target proteins were probed using SuperSignal West Pico Chemiluminescent Substrate (Thermo Fisher Scientific). ImageStudioLite software was used for quantification.

miRNA target prediction

Putative mRNA targets for individual miRNA were identified using TargetScan (http://www.targetscan.org/mmu_72/). The putative mRNA targets were crossed referenced in TargetScan and only the targets with conserved seed sequences were used for further confirmation with dual luciferase assay.

Plasmid constructions

3′-UTR containing the putative miRNA target sequences were either amplified by PCR or synthesized (Integrated DNA Technology) and subcloned into psiCHECK2 (Promega). The cDNA clone used for PCR were: mouse *Trib2* (IMAGE clone ID: 5363174), mouse *Mbnl1* (IMAGE clone ID: 6442315), and mouse *Slc25a42* (IMAGE clone ID: 5137229). Synthetic fragments of 500 base-pairs covered for the putative miRNA target site of *Gga3*, *Klf11*, *Ubap2*, and *Cyp26b1* were ordered from Integrated DNA Technology (IDT). Q5 site-directed mutagenesis kit (NEB Biolab) was used to mutate putative miRNA target sequences and verified by Sanger sequencing. Two tandem copies of sequences that were revered complement to the miRNA were subcloned into psiCHECK2 to generate miRNA sensors and verified by Sanger sequencing. The plasmids generated in this study were listed in key resources table.

Cell culture, miR-mimic treatment, dual luciferase assay

Flp-In TRex-HeLa cells[52,106] and Neuro2a[42] were maintained in DMEM with 10% FBS (Hyclone) and 1% Pen/Strep (Gibco) at 37°C and 5% atmospheric CO_2. Cells were seeded at 96-well plate in a density of 18,000 cells per well. Either miRNA mimics or control mimics were transfected at 30 nM together with the dual luciferase construct (sensor, wild type or seed mutant) per well using Lipofectamine 2000 (Thermo Fisher Scientific, E2940) following manufacturer's protocol. The effectiveness of miRNA-mediated knockdown is assayed with dual luciferase assays following the manufacture's protocol (Dual-Glo Luciferase assay system, Promega, E2940).

Motor neuron differentiation from human induced pluripotent stem cells and enrichment

The following human induced pluripotent stem cell lines are used in this study: BJ-iPS (healthy control), 18a (healthy control), 29days (familial ALS, mutSOD1^{L144F}), 47a (familial ALS, mutTDP43 ^{G298S}), 19f (familial ALS, mutC9ORF72), sALS1 (sporadic ALS), and sALS3 (sporadic ALS). Human induced pluripotent stem cell lines were routinely cultured on Matrigel-coated dishes in MACS iPS-Brew media (Miltenyi Biotec) and passaged using ReLESR (Stem Cell Technologies) on a weekly basis. Pluripotent stem cells were differentiated toward the spinal motor neuron fate following established protocols.[74] Briefly, pluripotent colonies were detached from the culture dish using Accutase and exposed

to neural induction media consisting of Neurobasal media, N2 supplement, NeuroBrew supplement, 4 μM CHIR99021 and 0.5 μM LDN-193189 for the first 10 days for culture on Matrigel-coated dishes. One μM Retinoic acid (RA) was supplemented into this media from days 3–10. From days 10–17, cells were cultured in motor neuron patterning media consisting of Neurobasal media, N2 supplement, NeuroBrew supplement, 1 μM RA and 1 μM Purmorphamine. Subsequently, from days 18–28, the adherent culture was dissociated into single cells and re-plated onto Matrigel-coated dishes in media consisting of Neurobasal media, N2 supplement, NeuroBrew supplement, 10 ng/mL BDNF and 10 ng/mL GDNF. Cells were treated with cytosine arabinoside (AraC) on Day 26 to kill off any proliferating cells for MN survival assay.

For baseline Trib2 levels, both healthy and ALS cultures were magnetically sorted on Day 28 using PSA-NCAM$^+$ and CD171$^+$ antibody (Miltenyi Biotec) to enrich MNs following manufacturer's protocol. Enriched MNs were then harvested for RNA analysis and RT-qPCR was done as described in the previous sections.

RNA interference and small molecule treatment in motor neuron cultures

Motor neuron cultures were dissociated with Accutase and seeded at 75,000 cells per well in a 96-well plate. Non-targeting siRNAs or siRNAs against genes of interest were individually complexed with Lipofectamine RNAiMAX (Invitrogen) following manufacturer's instructions. For each well, 20 nM of siRNAs and 1 μL of Lipofectamine RNAiMAX were used. Cells were harvested for RNA and protein analyses or fixed for immunostaining 3 days after siRNA transfection. RT-qPCR and immunoblotting analyses were done as described in the previous sections.

For small molecule treatment, TAK-285 and lapatinib was reconstituted in DMSO and diluted in media at the desired concentrations of 39 nM and 312 nM, respectively. Cells were harvested for RNA and protein analyses or fixed for immunostaining 3 days after small molecule treatment. RT-qPCR and immunoblotting analyses were done as described in the previous sections.

For miRNA mimics with small molecules treatment, the cells were treated with miRNA mimics for 24 h followed by small molecules for 48 h before harvesting. Non-targeting miRNA mimics or miRNAs against genes of interest were first individually complexed with Lipofectamine RNAiMAX (Invitrogen) following manufacturer's instructions. For each well, 25 nM of miRNAs and 1 μL of Lipofectamine RNAiMAX were used. After 24 h of transfection, cells were treated with TAK-285 and lapatinib at the desired concentrations of 39 nM and 312 nM for 48 h. Cells were harvested for RNA and protein analyses or fixed for immunostaining after small molecule treatment. RT-qPCR and immunoblotting analyses were done as described in the previous sections.

Immunofluorescence, image acquisition and image analysis of iPSC-derived motor neurons

Cells were fixed in 4% paraformaldehyde for 15 min, permeabilized in 0.1% Triton X-100 for 15 min and blocked in buffer containing 5% FBS and 1% BSA for an hour at room temperature. Primary antibodies were diluted in blocking buffer and incubated overnight at 4°C. The following antibodies (and their respective dilutions) were used: rabbit ISL1 (Abcam ab109517; 1:100), mouse SMI-32 (BioLegend 801701; 1:1000). The respective secondary antibodies (Molecular Probes, Invitrogen) were diluted at 1:1500 in blocking buffer and incubated at room temperature, in the dark, for 90 min. DAPI (0.1 μg/mL) to visualize cellular nuclei. Images were acquired using the high content microscope Opera Phenix (PerkinElmer) using the 20× air objective. Image analyses including cell counts and intensity measurements were performed using Columbus (PerkinElmer).

Immunohistochemistry, image acquisition and quantification, and immunoblotting using ALS patient tissues

Immunohistochemistry

Tissue sections from cervical and lumbar spinal cords were cut from blocks of formalin-fixed paraffin embedded ALS tissue (n = 10) and control tissue (n = 10), obtained from Dr. John Ravits' bank collection. Six μm-thick tissue sections were de-paraffinized through histology grade CitriSolv (two times for 15 min each) and a graded alcohol series (100, 90 and 70% ethanol (v/v) for 5 min each). After a 20 min permeabilization step in 1 × PBS, 0.2% Triton X-100, antigen retrieval 1% Tris-based (Vector Laboratories, H-3301) in pressure cooker at 120°C for 20 min, was applied to the sections. Sections were further blocked with 2% Fetal Bovine Serum (v/v, Atlanta Biologicals S11150) and incubated with Trib-2 antibodies (1:50; Proteintech #15359-1-AP) overnight at 4°C.

After that, sections were washed three times in PBS 1X and blocked with 2% Normal Donkey Serum (Millipore S30-100 mL) before incubation with secondary antibodies in PBS, 2% Normal Donkey Serum (v/v). After 60-min incubation with secondary antibody (Immpress reagent kit, anti-Rabbit, Vector) in room temperature, signals were detected using NovaRed (Vector, Sk-4800) for 1–5 min. Counterstaining was performed with hematoxylin (Fisher, HHS128). Imaging was performed on a Nanozoomer confocal microscope at the UCSD microscopy core.

Visualization and quantification

For IHC visualization, all slides were scanned with Hamamatsu Nanozoomer 2.0HT Slide scanner. With the use of NDP. view 2 viewing software, scanned slides were evaluated at 20× magnification. We selected the anterior horn areas, evaluated all the neurons in each tissue and determined the intensity of Trib2 expression in each neuron using Fiji. We did a color deconvolution choosing "H DAB" as the stain and define and from the 3 images we measured and quantified neurons in "Color_2" image since it is the staining without the counterstaining (Color_1 is the hematoxylin image). After determine the region of interest as was each neuron we used the "Mean gray value" as quantification in units of intensity. To convert the intensity numbers in Optical Density (OD) numbers we used the following formula: OD = log (max intensity/Mean intensity), where max intensity = 255 for 8-bit images. This quantified the average darkness of the image due to DAB signal.

Statistics

For analysis of datasets we employed a paired T-test and Mann Whitney test, a test for comparing non-parametric data. All data analyses and graphing were performed using the GraphPad Prism version 8.00 for Mac (GraphPad Software, La Jolla, CA).

METHOD DETAILS: QUANTIFICATION AND STATISTICAL ANALYSIS

All experiments using mice and cells, including Immunoblotting, immunofluorescence (IF), are representative of at least three independent experiments. GraphPad and R package were used for statistical analysis. ImageJ and Imaris software were used for image analysis. Statistical tests, parameter and quantification details, including n, SD/SEM, and p value, are reported in the corresponding figure legends and methods. The followings are denoted for p value: ns: not significant, #: $p < 0.10$ (with reporting p value), *: $p < 0.05$, **: $p < 0.01$, ***: $p < 0.001$, ****: $p < 0.0001$. Data distribution was assumed to be normal, but this was not formally tested.